

VARIABILITY PROPERTIES OF 4 MILLION SOURCES IN THE *TESS* INPUT CATALOG OBSERVED WITH THE KILODEGREE EXTREMELY LITTLE TELESCOPE SURVEY

RYAN J. OELKERS^{1*}, JOSEPH E. RODRIGUEZ², KEIVAN G. STASSUN^{1,3}, JOSHUA PEPPER⁴, GARRETT SOMERS¹, STELLA KAFKA⁵, DANIEL J. STEVENS⁶, THOMAS G. BEATTY^{7,8}, ROBERT J. SIVERD⁹, MICHAEL B. LUND¹, RUDOLF B. KUHN¹⁰, DAVID JAMES¹¹, B. SCOTT GAUDI⁶

Accepted for Publication in the Astronomical Journal

ABSTRACT

The Kilodegree Extremely Little Telescope (KELT) has been surveying more than 70% of the celestial sphere for nearly a decade. While the primary science goal of the survey is the discovery of transiting, large-radii planets around bright host stars, the survey has collected more than 10^6 images, with a typical cadence between 10 – 30 minutes, for more than 4 million sources with apparent visual magnitudes in the approximate range $7 < V < 13$. Here we provide a catalog of 52,741 objects showing significant large-amplitude fluctuations likely caused by stellar variability and 62,229 objects identified with likely stellar rotation periods. The detected variability ranges in *rms*-amplitude from 3 mmag to 2.3 mag, and the detected periods range from ~ 0.1 days to $\gtrsim 2000$ days. We provide variability upper limits for all other ~ 4 million sources. These upper limits are principally a function of stellar brightness, but we achieve typical 1σ sensitivity on 30-minute timescales down to ~ 5 mmag at $V \sim 8$, and down to ~ 43 mmag at $V \sim 13$. We have matched our catalog to the *TESS* Input catalog and the AAVSO Variable Star Index to precipitate the follow up and classification of each source. The catalog is maintained as a living database on the Filtergraph visualization portal at the URL https://filtergraph.com/kelt_vars.

1. INTRODUCTION

Technological advancements in the past two decades have led to a dramatic rise in the number of cost-effective, small-aperture, wide-field surveys which monitor large portions of the celestial sphere on a nightly basis. While antecedent astronomical observing strategies typically involved dozens of observations of a single star per night, contemporary surveys can obtain > 100 observations for $> 10^5$ sources on a nightly basis. These surveys have led to a number of discoveries in the fields of transiting exoplanets, supernovae, transient phenomena and variable stars (Bakos et al. 2004; Pollacco et al. 2006; Pepper et al. 2007; Basri et al. 2011; Pepper et al. 2012; Bakos et al. 2013; Law et al. 2013; Wang, L. et al. 2013; Oelkers et al. 2016a). These surveys have been particularly helpful to advance the techniques used in the reduction

and collection of massive amounts of astronomical data on practical timescales.

The first generation of time-series photometric surveys contributed to the discovery, catalog and study of nearly every type of known classical variable star and pioneered the methods for identifying variable stars used by modern surveys. Perhaps the most well known is the General Catalogue of Variable Stars (Samus' et al. 2017, GCVS), which has cataloged a variety of bright variables stars, distributed across the entire sky, since 1948. The All Sky Automated Survey (Pojmanski 1997, 2002, 2003; Pojmanski & Maciejewski 2004, 2005; Pojmanski et al. 2005, ASAS) and the Northern Sky Variability Survey (Woźniak et al. 2004b, NSVS) contributed to the basic understanding of the fundamental physics behind RR Lyraes (Kinemuchi et al. 2006; Szczygieł et al. 2009), β Cephei-types (Pigulski & Pojmański 2008), classical Cepheids (Pietrukowicz 2001), long-period variables (Woźniak et al. 2004a) and eclipsing binaries (Pilecki et al. 2007). Additionally, these survey aided in the precovery of numerous variables which would be observed by future space missions (Pigulski & Pojmański 2008).

Recently, the next generation of high cadence, time-series photometric surveys have led to the discovery of numerous interesting variable stars such as Blazhko effect RR Lyraes (Wang, L. et al. 2011), an eclipsing binary with a 70 year period (Rodriguez et al. 2016b), Type-II Cepheids in eclipsing systems (Wang, L. et al. 2013; Oelkers et al. 2015), and some yet to be explained phenomena (Boyajian et al. 2016). The Transiting Exoplanet Survey Satellite (hereafter, *TESS*) and Large Synoptic Survey Telescope (hereafter, LSST), which plan to survey nearly the entire celestial sphere expect to compound these discoveries (Ivezic et al. 2008; Ricker et al. 2014).

High cadence, time-series, photometric observations have also led to a shift in the definition of variability

¹ Department of Physics and Astronomy, Vanderbilt University, 6301 Stevenson Center, Nashville, TN 37235, USA

² Harvard-Smithsonian Center for Astrophysics, 60 Garden St, Cambridge, MA 02138, USA

³ Department of Physics, Fisk University, 1000 17th Avenue North, Nashville, TN 37208, USA

⁴ Department of Physics, Lehigh University, 16 Memorial Drive East, Bethlehem, PA 18015, USA

⁵ American Association of Variable Star Observers, 49 Bay State Rd., Cambridge, MA 02138, USA

⁶ Department of Astronomy, The Ohio State University, Columbus, OH 43210, USA

⁷ Department of Astronomy & Astrophysics, The Pennsylvania State University, 525 Davey Lab, University Park, PA 16802

⁸ Center for Exoplanets & Habitable Worlds, Pennsylvania State University, 525 Davey Lab, University Park, PA 16802

⁹ Las Cumbres Observatory Global Telescope Network, 6740 Cortona Dr., Suite 102, Santa Barbara, CA 93117, USA

¹⁰ South African Astronomical Observatory, PO Box 9, Observatory 7935, South Africa

¹¹ Astronomy Department, University of Washington, Box 351580, Seattle, WA 98195, USA

* Corresponding Author: ryan.j.oelkers@vanderbilt.edu

among stars. Observations using the *Kepler* space satellite provided nearly continuous monitoring of more than 10^5 stars for more than 4 years (Borucki et al. 2010). While the primary science goal of the satellite was the detection of transiting exoplanets, the telescope provided unprecedented and exquisite data, beneficial to a variety of stellar astrophysics. In particular, the high cadence measurements disputed the previous binary definition of a variable star: either a star is variable or it is “constant”. Instead, variable star classification now identifies *how much* variability a star exhibits, particularly on different timescales (Basri et al. 2011; Bastien et al. 2013; Ciardi & Howell 2017).

The Kilodegree Extremely Little Telescope (hereafter, KELT) has been providing high cadence, time-series photometry for more than 4 million sources since 2007. KELT observations have surveyed more than 70% of the celestial sphere, down to a limiting magnitude near $V \sim 13$, with a baseline of 9 yrs using KELT North (hereafter, KELT-N) and 5 yrs using KELT South (hereafter, KELT-S). Initially deployed to detect exoplanet transits around bright ($V < 10$) stars, the survey has contributed discoveries to supernovae (Siverd et al. 2015), the monitoring of Be Stars (Labadie-Bartz et al. 2017), eclipses of stars by disks (Rodriguez et al. 2013), gyrochronology of young stars (Cargile et al. 2014), pre-identification of young variable objects to be observed by K2 (Rodriguez et al. 2017a,b; Ansdell et al. 2017), more than 21 confirmed transiting planets (with 19 in press (Beatty et al. 2012; Pepper et al. 2013; Collins et al. 2014; Bieryla et al. 2015; Fulton et al. 2015; Eastman et al. 2016; Kuhn et al. 2016; Rodriguez et al. 2016c; Zhou et al. 2016; Gaudi et al. 2017; McLeod et al. 2017; Oberst et al. 2017; Pepper et al. 2017; Stevens et al. 2017; Temple et al. 2017; Lund et al. 2017; Siverd et al. 2017)) and 1 short period, transiting brown dwarf (Siverd et al. 2012).

This work represents the first comprehensive, full catalog search for variable sources observed by KELT. Our methodology can be useful in identifying variable sources in upcoming all sky surveys, such as with *TESS* or the Large Synoptic Survey Telescope (Ivezic et al. 2008). More immediately, the variability properties, amplitudes, and upper limits provided here for ~ 4 million stars in the *TESS* Input Catalog provide the community a means to optimize selection of interesting *TESS* targets (Stassun et al. 2017). The accessibility of the catalog through the Filtergraph visualization portal also allows for easy access to the stellar parameters for each source to aid in target follow up. The remainder of the paper is organized as follows: § 2 describes the KELT instrumentation, basic photometric pipeline and sources of survey noise; § 3 describes the search for variability and periodicity; § 4 describes our results; § 5 provides a brief discussion of additional applications of this work and the caveats associated with our catalog; and § 6 summarizes our conclusions.

2. THE KELT SURVEY

The KELT instruments were designed using many off-the-shelf components and software packages to speed development and ease possible maintenance (Pepper et al. 2007). Both KELT-N and KELT-S have the same basic set-up and components: a CCD detector, a medium-format camera lens, a photographic filter and a robotic

telescope mount. The instrumentation and data handling has been described in detail in Pepper et al. (2007, 2012) and we provide a summary of each instrument below.

2.1. KELT Instrumentation

2.1.1. KELT North

The KELT-N survey instrument includes an Apogee AP16E camera with a 4096×4096 , $9\mu\text{m}$ pixel Kodak KAF-16801E front-illuminated CCD. The detector can be thermo-electrically cooled to a temperature of $\Delta T \sim -30^\circ\text{C}$ relative to ambient but is set to maintain a constant -20°C . Testing of the CCD showed a dark current of $0.1\text{--}0.2\text{e}^- \text{pix}^{-1}\text{s}^{-1}$. The optics include a Mamiya 645 80 mm f/1.9 lens (42 mm effective aperture) and a Kodak Wratten #8 red-pass filter. The pixel scale of the detector is $\sim 23'' \text{pix}^{-1}$ leading to a total field of view (hereafter FoV) of $26^\circ \times 26^\circ$.

The KELT-N telescope has been observing from Winer Observatory in Sonoita Arizona ($31^\circ 39' 56.08''$ N, Longitude $110^\circ 36' 06.42''$ W, elevation 1515.7 m) since 2007. Winer Observatory hosts weather with 60% observable nights, half of which are determined to be photometric¹³.

2.1.2. KELT South

The KELT-S instrument is a near replica of the KELT-N instrument and includes an Apogee Alta U16M camera with a 4096×4096 , $9\mu\text{m}$ pixel Kodak KAF-16803 front illuminated CCD. The detector can be thermo-electrically cooled to a temperature of $\Delta T \sim -70^\circ\text{C}$ relative to ambient but is set to maintain a constant -20°C . Testing of the CCD showed a dark current of $< 0.26\text{e}^- \text{pix}^{-1}\text{s}^{-1}$. The optics include a Mamiya 645 80mm f/1.9 lens (42 mm effective aperture) and a Kodak Wratten #8 red-pass filter. The pixel scale of the detector is $\sim 23'' \text{pix}^{-1}$ leading to a total field of view (hereafter FoV) of $26^\circ \times 26^\circ$.

The KELT-S telescope has been observing from South African Astronomical Observatory near Sutherland South Africa ($32^\circ 22' 46''$ S, $20^\circ 38' 48''$ E, altitude 1768 m) since 2012. The Sutherland site typically experiences 70% observable nights with 60% of this time considered photometric. Typical seeing at the site reaches $\sim 0.92''$ ¹³.

2.2. KELT Observations

All KELT observations are robotic and do not require real-time human intervention for operations. The telescope control scripts undergo a variety of observability testing prior to the start of normal operations, including: checks on air temperature ($> -10^\circ\text{C}$); humidity ($< 90\%$); dew point; wind speed (< 60 km/h); precipitation and clouds. Bias frames and sky flats are taken first, and survey observations begin at astronomical twilight (Pepper et al. 2007, 2012).

Exposures are kept to 150 seconds (with a typical read-out time of 30 seconds) to optimize the photometric precision of stars with $8 < V_K < 10$, where V_K represents the zero-pointed KELT band pass to V magnitude. Each telescope typically targets a number of fields on any given

¹³ The seeing conditions are not a factor in observation quality given the large KELT pixel scale of $23'' \text{pix}^{-1}$.

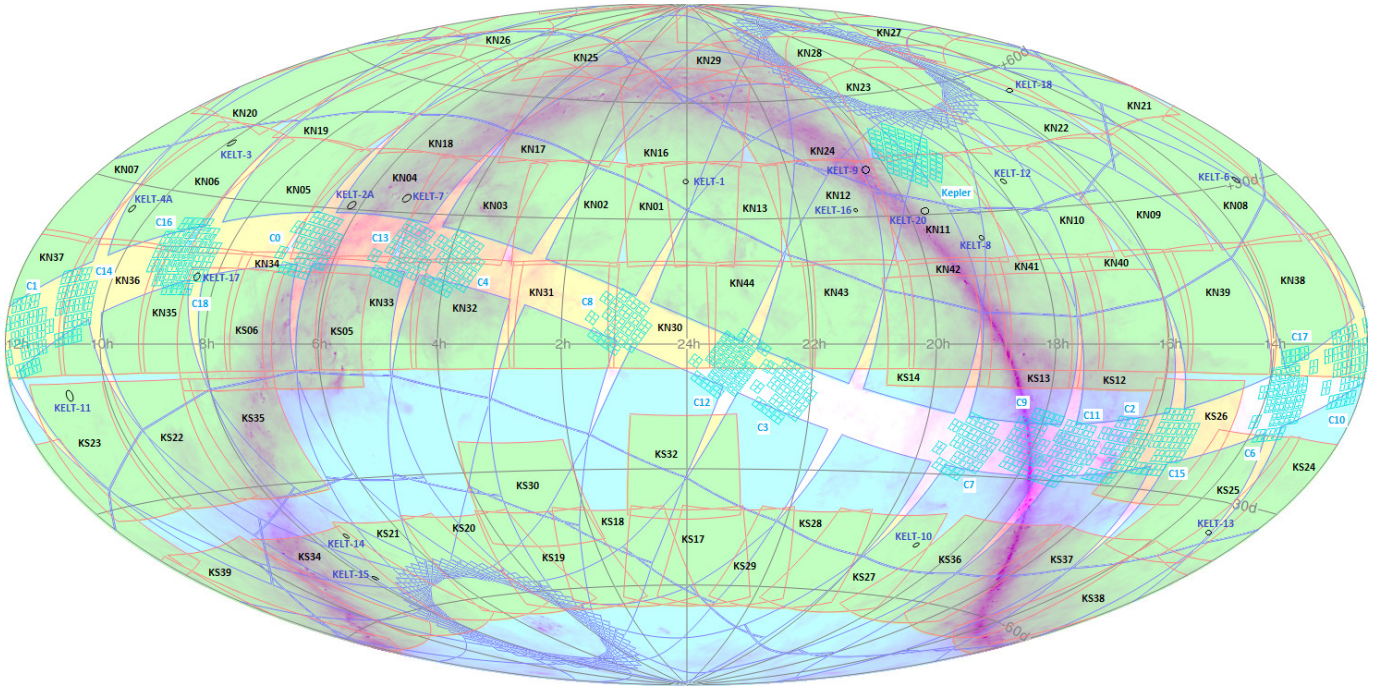


FIG. 1.— The complete field map for the KELT Survey (green tiles) with *TESS*, *Kepler* and *K2* footprints overlaid (blue tiles). The *TESS* fields are only for visualization purposes and the final placement may change. The Galactic plane is shown as a magenta stripe. The KELT survey fields used in this analysis are described in Table 1.

night, if the field is above 1.5 airmasses and typically further than $45^\circ - 55^\circ$ of the Moon (for KELT-S and KELT-N respectively). If a field is observable, it can be expected to receive 10-15 observations per night but can be as many as 30-50 depending on the location of the Moon. (Siverv et al. 2012; Kuhn et al. 2016) Figure 1 shows each KELT field and their location on the celestial sphere.

2.3. KELT Photometry

2.3.1. Image Processing and Flux Extraction

KELT-N images are pre-processed by undergoing dark subtraction, bias subtraction and flat fielding. The images are flat fielding using a master flat created from thousands of sky-flats, which have been individually bias-subtracted, dark subtracted and gradient corrected. KELT-N also creates a new master bias and master dark frame for each observing night. And the images are also 2D-calibrated using their night-specific master calibrations (Siverv et al. 2012).

KELT-S images are pre-processed by undergoing dark subtraction and flat fielding. The process uses a master dark and master flat-field. The master dark frame was created from hundreds of dark frames taken at the start of survey operations. The master flat frame was created using hundreds of sky-flats, which have been individually bias-subtracted, dark subtracted and gradient corrected (Pepper et al. 2012; Kuhn et al. 2016).

The KELT photometric pipeline uses a heavily modified version of the ISIS difference imaging routine (Alard & Lupton 1998; Alard 2000; Siverv et al. 2012; Kuhn et al. 2016). The reference frame for each field was created through an iterative rejection process to construct a frame using only high quality images taken at low air-

mass¹⁴ and low background signal.

The kernel used in the subtraction routine is constructed from a series of Gaussian functions and blurs the reference frame to match the seeing conditions in each of the science images. The two frames are subtracted and the residual flux is measured on the subtracted images using PSF-weighted, aperture photometry. The reference flux is extracted using PSF photometry from the stand alone DAOPHOT II program and is matched to the ISIS output with an aperture correction (Stetson 1987; Siverv et al. 2012; Kuhn et al. 2016). Finally, the raw flux is converted to magnitude, the light curves are 3σ clipped to remove outlier data points. Each light curve is fully reproduced from the photometry files when a new KELT observing season is completed (Siverv et al. 2012; Kuhn et al. 2016).

The KELT telescopes use a German Equatorial mount and the observations described in § 2.2, involve a meridian flip (near 0 hour angle) as the field passes from east to west of the meridian. This means all KELT fields will have images which need to be rotated 180° relative to one another. Rather than rotate the images during pre-processing, each field is divided into 2 data sets, East and West (hereafter, E and W) because the telescope optics are not exactly axi-symmetric (Pepper et al. 2007, 2012).

2.3.2. Noise

The careful documentation of possible sources of uncertainty is necessary to claim the detection of astrophysical signals. Flat-fielding errors, sub-optimal image alignments, poor subtractions and sub-optimal observing conditions can create possible sources of contamination

¹⁴ Not all fields can be observed at an airmass of 1, based on the latitude placement of the telescopes. But the reference frame selection, chooses images with the highest available transparency.

in photometry. While the KELT data goes through a rigorous set of data quality checks, these checks do remove all of the sources of uncertainty.

We compared the KELT photometric scatter to the noise limits expected from typical sources of astrophysical uncertainty: the photon count from a star, typical sky background levels and the scintillation limit. We modelled the statistical uncertainty as:

$$\sigma^2 = I_N^2 + (A \cdot I_{sky})^2 + \sigma_a^2 \quad (1)$$

where I_N and I_{sky} are the photon counts from the star and sky, respectively, A is the area of the photometric aperture, and σ_a is the scintillation limit defined by Young (1967) and Hartman et al. (2005) as:

$$\sigma_a = S_0 d^{-\frac{2}{3}} X^{\frac{7}{4}} e^{-\frac{h}{8000}} (2t_{ex})^{-\frac{1}{2}} \quad (2)$$

where S_0 is 0.1 when the diameter is defined in cm, d is the diameter of the telescope in cm, h is the altitude of the observatory, X is the airmass and t_{ex} is the exposure time in s. We approximate the expected noise using the values for KELT-N at Winer Observatory: $d = 4.2$ cm, $h = 1515$ m, $2 > X > 1$ and $t_{ex} = 150$ s. We find the scintillation limit to be $\approx 2 - 6$ mmag, depending on airmass. We measured the root-mean-square of the magnitude (hereafter, rms) of each light curve for the KELT-N05 field and compared those values with the noise model as a check of KELT’s basic photometric quality as shown in Figure 2. We find satisfactory agreement with the simple model described above, with the KELT system achieving typical rms of $1 - 2 \times$ the scintillation limit for stars with $V_K < 10$.

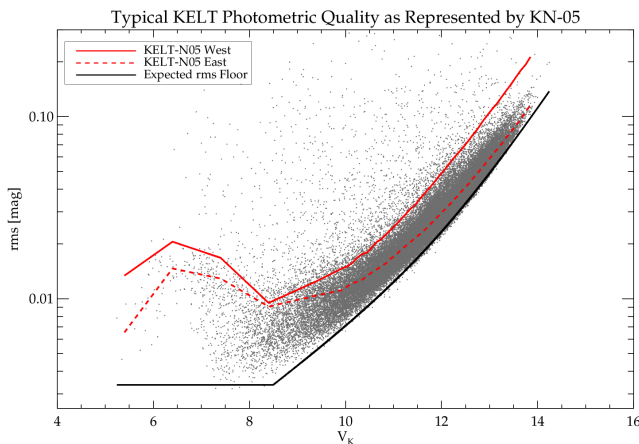


FIG. 2.— The minimum achieved rms , in magnitude, between the E and W orientations for the KELT-N05 field (grey points) as a function of KELT magnitude (converted to V magnitude). The solid red line represents the median rms for light curves observed when the telescope was in the W orientation and the dashed red line represents the median rms for light curves observed when the telescope was in the E orientation. The solid black line is the expected precision using the noise model described in § 2.3.2 assuming $X = 1.5$ and the sky background of the master frame. The noise model levels out around the expected scintillation limit of ~ 3.5 mmag. The rms increases near $V \approx 8$ as the number of counts on the detector reaches the saturation limit. We find the floor of the KELT light curve precision is in satisfactory agreement with our noise expectation for the system.

3. SEARCHING FOR VARIABILITY AND PERIODICITY

We objectively determine a KELT object’s variability with two methods, following the work of Wang, L. et al. (2013); Oelkers et al. (2015, 2016b). First, we employ 4 variability metrics designed to identify moderate-to-large scale variability which could be aperiodic or subtly occur over the large KELT baseline ($> \sim 5$ yrs), such as a steady decrease or increase in magnitude due to long term variation. Second, we impose 4 periodicity requirements designed to identify small-to-large scale variability which repeats on periodic timescales and is *not* consistent with frequencies of common KELT systematics.

These metrics are used to discover variable and periodic objects in the KELT survey on a per field basis and assume, in general, most stars will *not* be variable but “constant”. Each metric is calculated on a per star basis and the values are compared with either the entire sample or a subset of each sample with similar magnitude (± 0.5 mag). We find by employing these metrics in this way, we greatly reduce contamination by systematics (due to poor subtractions or observing conditions) because “constant” stars in the same field, with similar magnitudes, should have similar dispersions, even if affected by systematics. Additionally, we emphasize these metrics are empirical in nature, and while they reasonably identify true variable stars and eliminate false positives, the specific selection criteria described in § 3.1 and 3.2 are ultimately subjective, *not* statistical, and may need to be updated for other data sets.

As previously mentioned, KELT has two orientations per field: E and W. We searched each field orientation independently and compared the results for objects in both orientations. If the star had a light curve in both orientations but was only determined to be variable in one, the star was rejected as a variable¹⁵. This was done under the assumption that if a star is an *bona-fide* variable, it should show similar variations in both the E and W orientations since true astrophysical variability will be independent of the telescope’s position relative to the meridian.

3.1. Variability Testing

First, we identify stars where the dispersion in their light curves is larger than is expected for stars of similar magnitude in the KELT band-pass. For this analysis we use 2 metrics: the rms and the Δ_{90} metric. The rms metric identifies the magnitude range for 68% of the data points in each light curve and the Δ_{90} metric identifies the magnitude range for 90% of the data points in each light curve (Wang, L. et al. 2013). We compute the upper $p < 0.05$ envelopes of both statistics, as a function of magnitude, and assume any object lying above these limits is a *bona-fide* variable. Neither metric is calculated using error weighting, but because we wanted the envelopes to be based on “constant” stars¹⁶, we applied a 3σ iterative clipping to the rms and Δ_{90} metric values, in each magnitude range, prior to calculating the envelope.

Next, we compute the Welch-Stetson J and L metrics (Stetson 1996). These two metrics are useful in identifying significant, correlated variations between subsequent

¹⁵ If a star only had a light curve in 1 field but passed the tests below, it was included in the variable data set but appropriately flagged, see § 3.3

¹⁶ We define “constant” stars as objects displaying dispersion similar to *most* stars of the same magnitude.

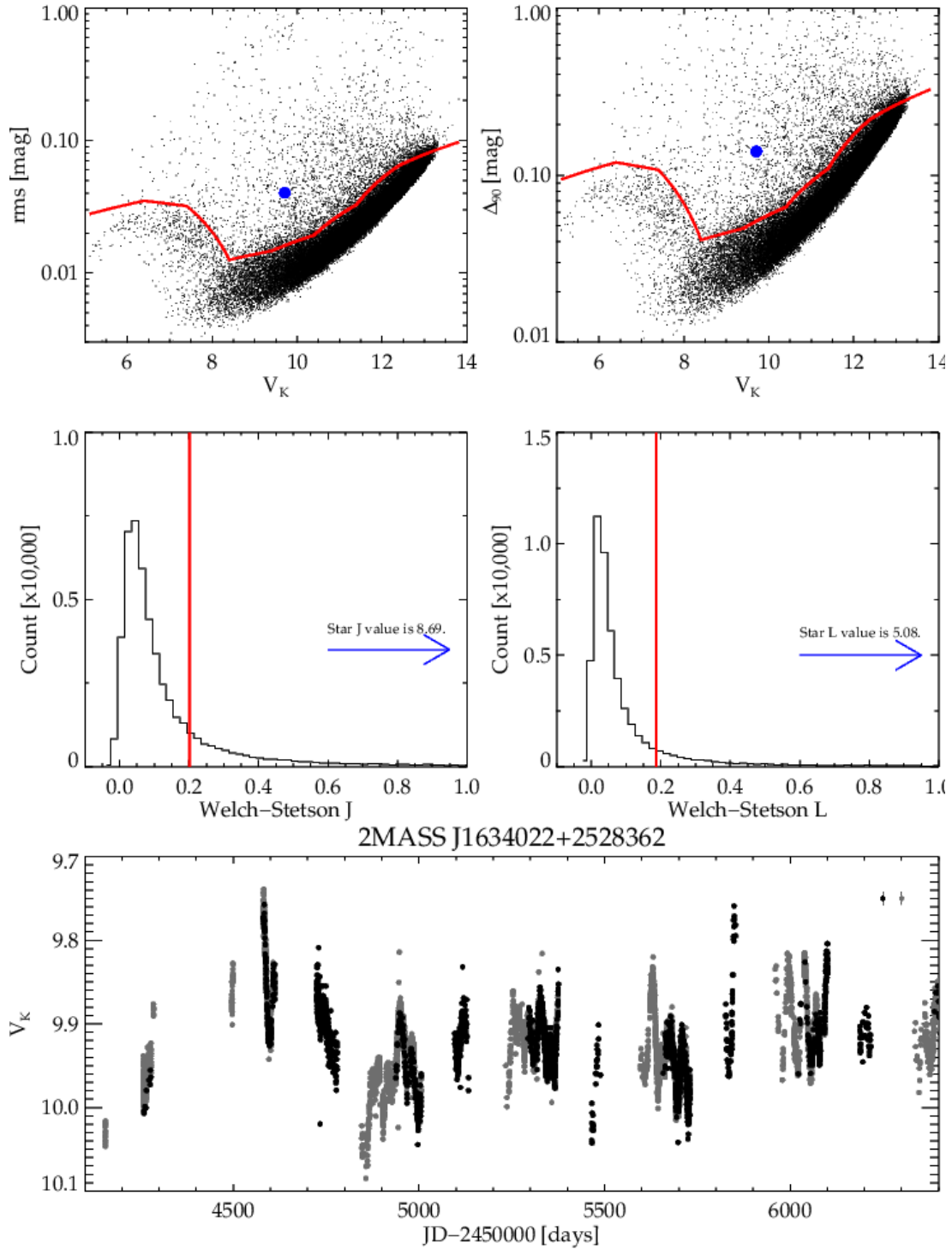


FIG. 3.— The variability metrics used to identify stars with large amplitude changes relative to the ensemble set of light curves in each orientation of KELT-N10. For clarity only the results for the W orientation are shown. In practice the star must pass all 4 metrics in *both* the E and W orientations to be considered variable. The red lines denote the cut-offs in each panel and the blue dots or arrows represent the value of the star show in the bottom panel. *top left*: the *rms* metric; *top right*: the Δ_{90} metric; *middle left*: the Welch-Stetson J metric; *middle right*: the Welch-Stetson L metric; *bottom*: combined E (grey points) and W (black points) orientation light curves for the variable object J1634022+2528362. Typical photometric error is shown at the top right of the panel.

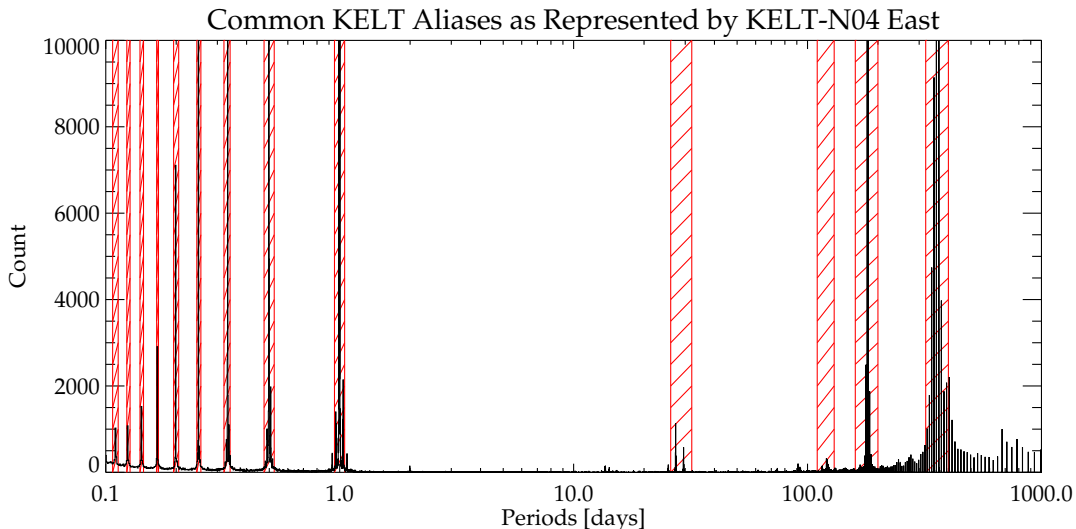


FIG. 4.— A histogram of the top 5 periods of all KELT stars in the E orientation of KELT-N04. Large peaks in the histogram (generally where > 500 stars having a similar period) denote artificial periods caused by the observing cadence of the survey. The hashed red areas represent the periods most likely to be caused by aliasing of the KELT observational cadence, the lunar cycle, the solar day and the calendar year. These regions are masked in our analysis (see § 3.2). Any candidate period recovered in one of the hashed red areas is *not* considered an astrophysical candidate period. A candidate period (P) is also not considered astrophysical if the period’s first 2 harmonics ($2P$, $3P$) or sub-harmonics ($P/2$, $P/3$) fall in any of the hashed, red areas.

data points with the sampling rate of KELT: typically 10–30 min. These metrics are expected to produce a distributions centered at or near zero with a one-sided tail. Stars in this tail represent significant deviations likely not to be caused by systematics. We compute the $p < 0.003$ cutoff of this tail in both J and L to select variable objects.

We initially remove objects with $J, L > 10$ and do a 3σ iterative clipping determine the mean and standard deviation of the J and L distributions because we are interested in our metric cut-offs being based on “constant” stars¹⁶. This clipping allows us to calculate the distribution properties of J and L using a population of stars which show minimal deviation between subsequent data points.

Additionally, we found the J statistic to be much more sensitive to systematics caused by detector saturation. This caused some objects to have very large J values and small-to-moderate relative L values. Therefore, we made a final requirement that the ratio of J -to- L must not be greater than 1.5.

Figure 3 shows the 4 variability metrics recovering a variable star in W orientation of KELT-N10. The E and W light curves of the passing variable object, 2MASS J1634022+2528362, are also shown.

3.2. Periodicity Testing

We identify stars with significant periodic signals using the ASTROPY, python implementation of Lomb-Scargle (Lomb 1976; Scargle 1982). We searched each light curve for the top 5 periods, ranked by power, between 0.1 days and the total number of baseline days in a given KELT E or W field orientation. Periods were independently searched between the E and W orientations to help eliminate spurious signals. Again, we assume a *bona-fide* astrophysical period will be independent of telescope position. We required each period to pass the 4 requirements below, before we accepted the period as valid.

First, we required any candidate period to match

within 1% of the period in the other field orientation. For example, if the E light curve had a period of 1 day, then the W period must also have a period between 0.99 and 1.01 days. If the E period is 100 days, then the W period must be between 99 and 101 days and so on. If a star had a light curve in *only* the E or W data, this step is skipped but the star was appropriately flagged (see § 3.3).

Second, we required the period to be unique. This means no other candidate period returned by the Lomb-Scargle search can be identical to a period identified by Lomb-Scargle in the fourier spectrum of a different star in the same field-orientation. While we remove the most common observing aliases known in the KELT data (see below), each combination of field and orientation has a unique set of image timestamps and thus a unique spectral window function. As a result, the aliasing pattern varies from field to field. By requiring the periods to be unique, we help to alleviate this tension. However, if two stars showed identical periods in a given field *and* the stars were blended (within 5 KELT pixels of one another), we considered the period valid for both stars, but again, the stars are flagged (see § 3.3).

Third, we excluded periods near the following KELT aliases: the most common diurnal aliases (0.10 ± 0.003 d, 0.125 ± 0.002 d, 0.1425 ± 0.0025 d, 0.1665 ± 0.0015 d, 0.2 ± 0.005 d, 0.25 ± 0.025 d, 0.33 ± 0.01 d, 0.5 ± 0.025 days and 1 ± 0.05 d); the lunar month, 29 ± 3 d; roughly a third of a year 120 ± 10 d; roughly half a year, 180 ± 20 d; and roughly a calendar year 360 ± 40 days. Since many aliased peaks can be disguised as harmonics and/or sub-harmonics, we also checked if $P/2$, $P/3$, $2P$, or $3P$ would fail the alias check, and if so, we removed the period as suggested by previous studies (VanderPlas 2017). The regions of exclusion due to observing alias contamination are shown visually in Figure 4.

Fourth, we placed a limit on the normalized power, and only accepted periods with powers larger than 0.1

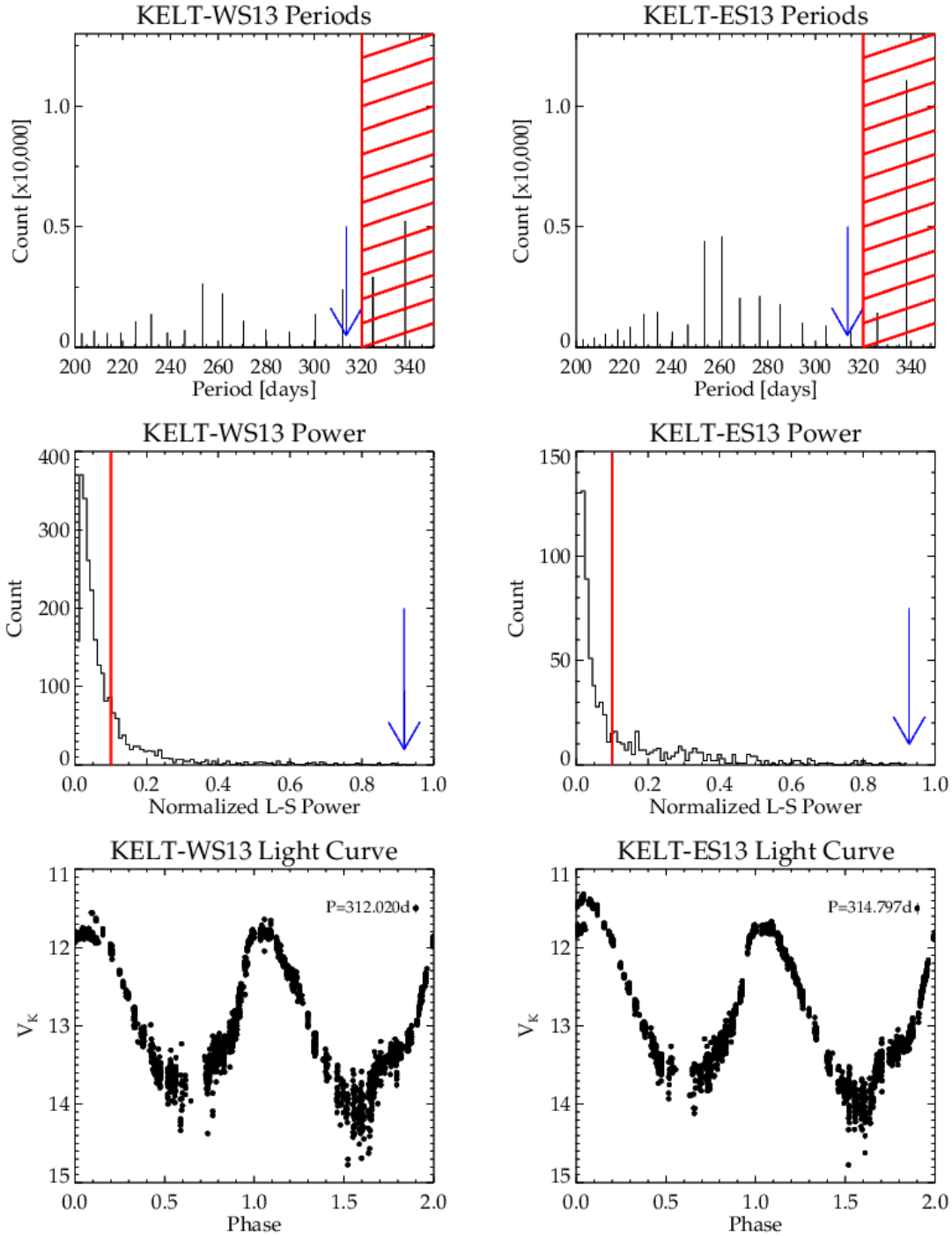


FIG. 5.— The periodicity requirements used to identify stars with *bona-fide* astrophysical periodicity. The blue arrows are used to denote the representative, periodic star 2MASS J17390451-0447289 ($P \sim 313.408$ d) passing each requirement. *Top Row:* Histograms of the top 5 peak periods for all stars, regardless of whether they pass the periodicity requirements in § 3.2, for the W (left) and E (right) orientations of KELT-S13. The alias cut-off for an approximate calendar year (360 ± 40 d) shown as a the hashed red region. Periods to the right of this line are likely aliases of the calendar year. *Middle Row:* The normalized L-S power for *every* stellar period recovered in the KELT-S13 analysis within $\sim 313 \pm 3.1$ days (1% of the candidate period). The candidate period’s normalized power is shown to be larger than both the average power and the 0.1 power requirement. *Bottom Row:* The phase folded light curve for 2MASS J17390451-0447289 in the W (left) and E (right) orientations. The star has been folded on twice the period and plotted for clarity. The star is clearly periodic, with the amplitude of the periodicity changing between cycles, which may indicate the true period is twice that of our detected period. Typical photometric error and the recovered period in each field orientation is shown at the top right of these panels.

as candidate astrophysical signals. Next, we identified all periods from all stars in a given KELT field orientation within the period range $P - (P \times 0.01) < P < P + (P \times 0.01)$, where P is the candidate period. We then calculated the mean power of these periods and compared this mean power, to the power of the candidate period. We required the candidate period’s power to be larger than the mean power. This metric was included to remove some spurious periods which were caused by aliases of signals other than the sidereal day, lunar month and calendar year but were found in multiple stars. This metric also helped to remove stars which were blended with nearby, *bona-fide* periodic stars, since the blended star’s power was typically much lower than the power of the periodic star.

Any period which satisfied these 4 requirements was considered to be genuine. Additionally, we consider a star to be multi-periodic if we could identify more than 1 period in a given light curve which satisfied the above requirements. Figure 5 shows the implementation of these 4 requirements for the representative periodic object, 2MASS J17390451-0447289, from the KELT field S13.

3.3. Identifying Possible Contamination from Non-Astrophysical Sources

While we take care to select objects most likely to be *bona-fide* variables, the catalog is not free from spurious members. We have created a set of 6 catalogs flags designed to educate the reader that a given variable *could* be contaminated by common KELT systematics. These catalog flags are described as:

1. EDGE: If a star was closer than 200 pixels to the edge of the CCD, the EDGE flag is set to 1.
2. POINTS: If the total number of data points for any light curve is less than $N < \mu_N - 1\sigma_N$, where N is the number of data points in the light curve, μ_N is the mean number of data points of all light curves in the E/W orientation and σ_N is the standard deviation of the mean number of data points per field, the POINTS flag is set to 1.
3. BLEND: If the centroid of a stars was within 5 pix (1.9’) of the centroid of another star brighter by more than 1.5 magnitudes, the BLEND flag is set to 1.
4. PROXIMITY: If a candidate variable is within 5 pix (1.9’) of another candidate variable, the PROXIMITY flag is set to 1.
5. ALIAS: If at least 3 of the top 5 peaks in the Lomb-Scargle power spectrum are aliases of the sidereal day, lunar month or calendar year the ALIAS flag is set to 1.
6. SINGLE: If a star has only 1 light curve (either E or W but not both) and passed either all variability metrics or periodicity requirements, the SINGLE flag is set to 1.

4. RESULTS

4.1. Variable and Periodic Sources in KELT

We identify 52,741 stars as variable or periodic using the metrics and requirements above. From this list, 35,060 stars passed all variability metrics; 21,362 stars passed all periodicity requirements; and 3,618 stars passed both the variability metrics and periodicity requirements. 15,072 stars passing the variability metrics have all contamination flags set to 0; 7,580 stars passing the periodicity requirements have all contamination flags set to 0; and 1,193 stars passing both the variability metrics and periodicity requirements have all contamination flags set to 0. Figure 6 shows the distribution of KELT variables across the celestial sphere.

Not surprisingly, the stars identified as having periodic signals have variations which can be both small-amplitude (< 0.1 mag) and large-amplitude (> 0.1 mag). The stars identified with the variability metrics tend to have larger amplitude variations as shown in Figure 7. This bias is expected since the variability metrics require relatively large amplitude variation to pass each metric.

We determine the variable star rate (V_r) in the Milky Way Galaxy as a function of Galactic latitude (b) by dividing the number of variables found in each field (N_V) by the total number of stars in a given field (N_{tot}) as shown by: $V_r = N_V/N_{tot}$. We find the variable star rate correlates with absolute Galactic latitude as shown in Figure 8. We find the variable star rate to be as much as 3% at low Galactic latitudes ($|b| < 20^\circ$) to a rate of 1% at higher Galactic latitudes ($|b| > 20^\circ$). These rates are consistent with the variable star rates determined by previous studies (Wang, L. et al. 2013; Díaz et al. 2016; Oelkers et al. 2016a,b).

Figures 9 and 10 shows example light curves for 18 stars passing the variability metrics from various KELT fields, while Figure 11 and 12 show example light curves for 18 stars passing the periodicity metrics from various KELT fields. The full catalog, including the cross matches described below, has been made available through the Filtergraph visualization portal (Burger et al. 2013) at the URL https://filtergraph.com/kelt_vars. Through this portal the public can access all variability information determined for the star; the cross matches with the *TESS* Input Catalog and AAVSO Variable Star Index (see § 4.3 and 4.4 for more details); and a basic light curve image for the W and E light curves. Additionally, we provide the catalog in normal table format with: Table 2 detailing the catalog and astrometric information for each variable; Table 3 detailing the magnitude information for each variable; and Table 4 detailing the variability metrics and catalog flags for each variable.

4.2. Variability Upper Limits for all Remaining Sources

The catalog described in § 4.1 was created to identify the *most* variable objects observed by KELT, which may also be observed by large scale photometric surveys in the future, such as the upcoming *TESS* mission. This method of pre-identification of variable objects KELT, prior to mission start, has been shown to work well for the K2 mission (Rodriguez et al. 2017a,b; Ansdell et al. 2017). However, we expect the catalog will not identify every variable object because either: (1) the statistics we applied were too strict for some variable objects to be re-

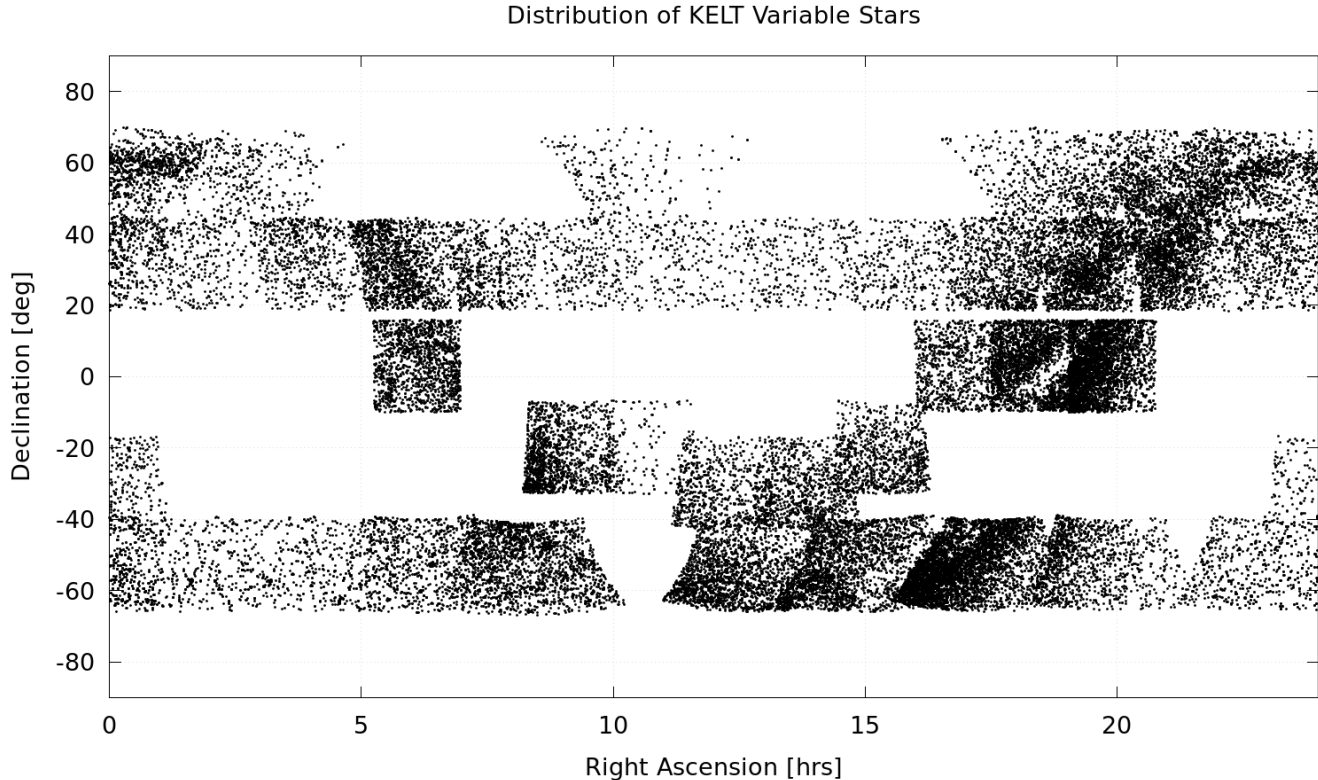


FIG. 6.— An all sky map of KELT variable stars. Clear over densities can be seen near the Galactic Plane.

covered even if they show considerable large amplitude variations; or (2) the star’s variability occurred below the typical KELT precision for a given star and could not be objectively differentiated from the expected system noise (see Figure 2). Given KELT has observed an additional 4 million objects, we believe we can use the remaining KELT catalog to provide additional variability information which may be useful for community members wishing to identify variable objects through their own independent metrics.

Therefore, we provide an upper limit for the variability for the remaining objects observed by the KELT survey. Table 5 provides the *rms* metric on times scales of 30 minute (similar to the expected 30 minute full-frame images provided by the *TESS* mission (Ricker et al. 2014)), 2 hours and 1 day. This catalog extension aims to provide the astronomical community with complete upper limits of all stars, not just those showing the most significant variability. We emphasize these statistics should only be interpreted as upper limits and will vary significantly with the star’s KELT magnitude.

4.3. Variability Properties of Stars in the *TESS* Input Catalog

TESS and KELT share many similarities in their design. Both telescopes have modest apertures (< 10 cm) and wide FoV ($26^\circ \times 26^\circ$)¹⁷. While efficient at surveying large portions of the celestial hemisphere quickly, this optical design leads to crowded sources and can make pin-pointing the source of variability cumbersome. Our

¹⁷ *TESS* will have 4 such $24^\circ \times 24^\circ$ FoVs per pointing, so the combined FoV per pointing will be larger than a KELT field.

variable catalog can lessen the burden of some variability detection by acting as precovery for many sources *TESS* is expected to observe.

We matched any star with a 2MASS identification in the KELT variable catalog to the fifth version of the *TESS* Input Catalog (hereafter, TIC). The TIC is an ambitious catalog which attempts to create a nearly uniform list of stellar parameters, such as effective temperature, mass and radius, for more than 470 million stars and is the primary source of target selection for the upcoming *TESS* mission (Ricker et al. 2014; Stassun et al. 2017). We provide the TIC Identification as part of our library and adopt the stellar parameters provided by the TIC, when available.

4.3.1. Searching for Large Amplitude Variability Among the top *TESS* 2-minute Target Candidates

We also compared our variable catalog with the specialized transiting Candidate Target List (tCTL) of the TIC. This list identifies the stars most suitable for searching for transit-like signals and provides a prioritized list of stars which may be included in the final list of 400,000 targets to receive 2-minute cadence during the *TESS* mission (Stassun et al. 2017). Because the detection of transit-like signatures is simplified when a light curve is quiescent, it would be preferable for stars in the final 400,000 member target list to show minimal stellar variations.

We found 493 objects identified in our catalog to be within the top $\sim 400,000$ tCTL candidate members and 3,339 being in the top 2,500,000 targets. While the increased cadence observations these variables could help diagnose the origin of their variability, future versions

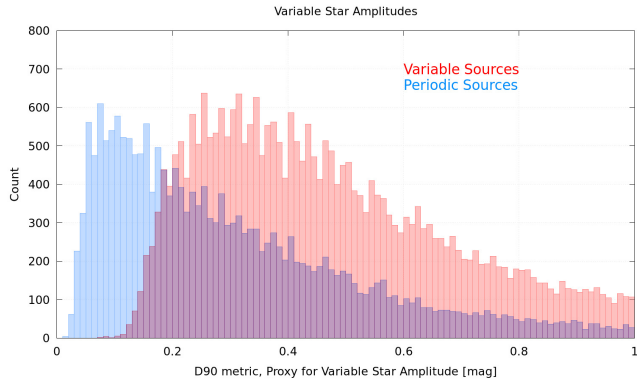


FIG. 7.— Comparison of the Δ_{90} metric (which is a proxy for the amplitude of variability) for stars which pass the variability metrics (red histograms) and stars which meet the periodicity requirements (blue histograms). The majority of stars, passing the variable metrics, have amplitudes larger than 0.1 mag. This bias is expected because the variability metrics are designed to identify stars with relatively large amplitude variability. The stars which pass the periodic requirements, while they require significant power in their power-spectrum, have no amplitude requirements for detection and can recover variable amplitudes much smaller than 0.1 mag.

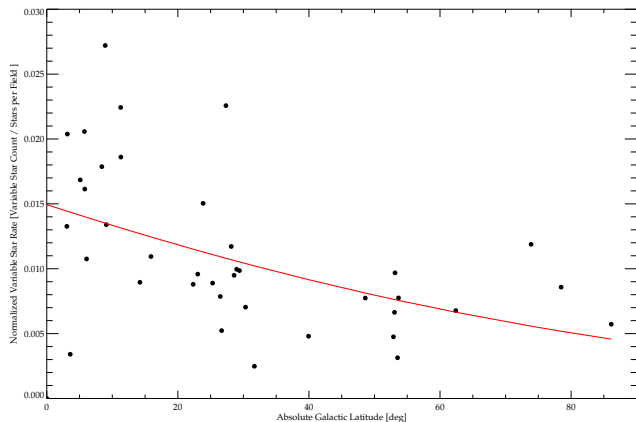


FIG. 8.— The normalized variable star rate as a function of absolute Galactic latitude. The normalized variable star rate is defined as $V_r = N_V/N_{tot}$, where V_r is the normalized variable star rate, N_V is the total number of variable stars in a given KELT field and N_{tot} is the total number of stars in a given KELT field. We find as Galactic latitude decreases, the number of variable star detections increases.

of the tCTL may benefit from a variability measure included in calculations of the star’s priority *if* the primary goal of the 2 minute science targets will be the detection of transiting Earth-sized planets. However, given the current number of identified variable stars in the tCTL is $< 1\%$, we do not expect variable stars to heavily contaminate this highly cultivated list.

4.3.2. A Focused Search for Rotation Periods of TESS Target Candidates in KELT Light Curves

Following the approach of Stassun et al. (1999), we also executed a search for periodic signals most likely to come from the rotation period of the star for a specific subset of KELT stars: those identified as high priority dwarfs expected to be observed in the *TESS* 2 minute cadence (Stassun et al. 2017)¹⁸. This search was designed to test

¹⁸ The TIC is meant to be a living catalog and is currently version 5. Some objects in this analysis may no longer be considered

the feasibility of recovering a rotation period from future *TESS* light curves given the basic designs of both systems are comparable in terms of expected pixel scale, crowding and blending effects.

For these stars, we combined the E and W light curves into a single light curve and post-processed the data using the Trend-Filtering Algorithm (Kovács et al. 2005) to remove common detector systematics. We searched for rotation signals in the combined light curves using a modified version of the Lomb-Scargle period finder algorithm (Lomb 1976; Scargle 1982). We searched for periods between a minimum period of 0.5 days and a maximum period of 50 days using 2000 frequency steps. Additionally, we masked periods between 0.5 and 0.505 days and 0.97–1.04 days to avoid the most common detector aliases associated with the solar and sidereal day and selected the highest peak of the power spectrum as the candidate period.

We then executed a boot-strap analysis, using 1000 Monte-Carlo iterations, where the dates of the observations were not changed but the magnitude values of light curve were randomly scrambled (see Henderson & Stassun 2012). We recalculated the Lomb-Scargle power spectrum for each iteration and recorded the maximum peak power. If, after 1000 iterations, a maximum power of the boot-strap analysis was found to be larger than the power of the candidate period, the period was rejected as a false-positive.

We identified 62,229 stars with possible rotation periods as defined in our search. Table 6 provides basic stellar parameters from the TIC and the rotation period information for each star. Of these stars, 2,110 were also found in the searches described in § 3.1 and § 3.2. However, the remaining $\sim 60,000$ stars were found to have rotation periods were not identified as part of these ensemble searches and $\sim 10,000$ periods from the ensemble search were not found as part of the rotation search.

These periods were likely not recovered in the ensemble period search for the following reasons. First, the ensemble period search was for $0.1 \text{ d} < P < \max(\text{baseline}) \text{ days}$, whereas the rotation search was limited to $0.5 < P < 50 \text{ days}$. The difference in the period range searched also resulted in some difference in the number and spacing of frequencies searched. Second, the ensemble search considered the E and W light curves separately in order to ensure the robust identification of truly significant variability, while the rotation search used the combined light curves to increase the rotation period signal. Because rotation periods are typically low amplitude, it is possible the ensemble search did not have enough power for the signal to reach the threshold of 0.1 in normalized power. Third, the ensemble search used the raw photometry and the rotation search used detrended photometry. Finally, the ensemble search greatly expanded the masked period regions and required unique periods, while the rotation search used a boot-strap analysis to determine the likelihood the period was genuine. More fundamentally, the ensemble analysis was intended to identify large-amplitude variations that meet stringent crite-

high priority dwarfs and other targets may have been added as our search began with version 3 of the TIC. However, all targets in this analysis are still identified in the TIC regardless of their priority status

ria for significance, whereas the rotation-focused analysis was designed to identify periodic signals that could in some cases be detected at amplitudes below that required by the rms , Δ_{90} , or Welch-Stetson J and L metrics.

4.4. Cross-Match with the AAVSO Variable Star Index

The American Association of Variable Star Observers (hereafter, AAVSO) has created and cultivated the Variable Star Index (hereafter, VSX) since 2006 (Watson 2006). The VSX combines basic variability and astrometric information for more than 400,000 variable stars discovered by both amateur and professional astronomers. We matched our catalog to the VSX, selecting the nearest variable within $30''$, and found 19,313 matches.

We compared the absolute difference between a given variable star’s magnitude at maximum and magnitude at minimum, as reported by the VSX, to serve as the variable star’s variable amplitude. We then compared this to our own proxy for variable amplitude, the Δ_{90} metric as shown in the top panel of Figure 13. While 726, or 12% of stars with reported maximum and minimum magnitude values, appear to have similar amplitudes in both catalogs, we find the majority of the stars VSX show larger amplitudes than reported in our catalog. This could be because the Δ_{90} metric is expected to under-estimate the true variable amplitude (since it is only the 90-th percentile magnitude range) but also because the KELT magnitude filter is a redish, broad pass band which may be dampening the variable amplitude which typically peak in the blue part of the electromagnetic spectrum.

We also compared our recovered periods and those listed in the VSX as shown in the bottom panel of Figure 13. We find that 3,564, or 56% of the periodic stars in both the VSX and our catalog, have similar periods or are aliases of the VSX period ($P/2$, $P/3$, $2P$, $3P$). Additionally, many of the periods recovered by our methods appear to be beat frequencies of the VSX period or vice-versa (shown as the parabolic features in the bottom panel of Figure 13 (Long et al. 2016; VanderPlas 2017)) helping to confirm these sources are likely true periodic variables.

4.5. Using Other Catalogs to Infer the Characteristics of KELT Variables

We can infer basic characteristics of the KELT variable data set using the information provided by the TIC. We select KELT periodic stars with periods < 100 days and valid parallax information. We then make a Hertzsprung-Russell diagram by transforming the observed K_S magnitude into an absolute K_S magnitude and calculate the $V - K_S$ color.

We find stars on the giant branch tend to have much slower rotation periods than stars on the main sequence (Fig. 14, top panel). This is expected for rotation periods of giant stars, as stars tend to spin down as they age (van Saders & Pinsonneault 2013; Tayar et al. 2015). Stars in the low-mass end of main-sequence also show longer rotation periods than their higher-mass counterparts, which could indicate the Kraft-break and would be expected for a typical field population (Kraft 1967). There are a few objects along the giant branch with short periods

and these are likely pulsators, such as RR Lyrae, or objects within short period eclipsing binary star systems. Phased light curves for three objects, from three parts of the HR diagram, can be seen in the bottom panels of Fig. 14.

Similarly, we created an HR diagram for stars which pass the variable metrics as shown in the top panel of Figure 15. We color this HR diagram heatmap by the sum of the Welch-Stetson J and L metrics. Here we find the sums tend to be larger (> 10) for objects identified as giants and sub-giants. Time-series light curves for 3 stars, from 3 separate regions of the HR diagram, are shown in the bottom part of Figure 15.

The Welch-Stetson J and L metrics were designed to identify objects which show variable behavior which is heavily correlated with time (i.e. objects with periodic and/or continuous variability) (Stetson 1996). The large metric values for stars on the giant branch could indicate correlated and continuous stellar variability increases with age, as expected for stars in the instability strips or the detection of possible seismic oscillations which can occur on timescales of 10-100 days. The smaller combined J and L values for dwarf stars also indicates the variability detected in these stars could be due to spot variation and rotation or sudden solitary variability, such as a stellar flare, rather than the large amplitude, continuous pulsations found in their giant counterparts.

5. DISCUSSION

5.1. Additional Applications of the KELT Variability and Periodicity Catalog

The long KELT baseline (5 – 9 years) also provides an opportunity to study the long term evolution of variable star behaviour. Observations with KELT¹⁹ and other long baseline surveys, such as KEPLER (Borucki et al. 2010), OGLE (Udalski et al. 1994) and WASP (Pollacco et al. 2006), have shown many variable objects tend to modify their variability as a function of time. Therefore, long baseline observations can provide scientific insight into previously unknown stellar astrophysics and phenomena.

Three variables with evolving behaviour, which could have been missed without the baseline of KELT, are shown in Figure 16. The top panel shows, 2MASS J05095273+3700158, also known as HD 33152. The star shows long term variability with a large (~ 0.5 mag) increase in magnitude between 2455000 – 2456000 days consistent with being a possible long period Be star (previously identified in Labadie-Bartz et al. (2017)) with the magnitude returning to its initial brightness near 2457000 days. Interestingly, this object appears to show large amplitude (0.1 – 0.4 mag) outbursts consistently during its brightening. The identification of these outbursts indicates the KELT survey could participate in a search for similar stellar flares and outbursts in other stars. Such a search could help to constrain flare rates for early-type dwarfs, which have been excluded from previous stellar flare studies which focused on late-type dwarfs in SDSS photometry, Kepler light curves and photometry from the Chinese Small Telescope Array (Kowalski et al.

¹⁹ Particularly those in the Disk Eclipsing Survey with KELT (hereafter, DESK) survey (Rodríguez et al. 2016a)

2009; Hawley et al. 2014; Oelkers et al. 2016b; Liang et al. 2016).

The middle panel of Figures 16 shows the recovery of the DESK object 2MASS J04181078+2591574, also known as V409 Tau (Rodriguez et al. 2015). The object is identified as a classical T-Tauri star which was shown to be occulted by a protoplanetary disk on an interval of nearly 600 days. Since the publication of Rodriguez et al. (2015), the star has shown yet another dimming event of similar duration $\sim 500 - 800$ days.

The bottom panel of Figure 16, shows 2MASS J15303924+3547043 also known as ST Boo. Our match with the VSX shows this star was previously identified as an RR Lyrae-type variable with a primary period of 0.622 days. When the time-series light curve of this variable is plotted, clear period doubling and amplitude modulation can be seen, indicative of the Blazhko effect (Blazhko 1907). While in recent years the cause of the Blazhko effect has better constrained (nearly 50% of RRab stars show the modulation; e.g., Jurcsik et al. 2009) the star’s relatively bright V magnitude at minimum, ≈ 11.35 , short pulsation period of 0.622 days and typical Blazhko modulation in < 100 days makes it an excellent candidate for further study.

5.2. Caveats and Future Directions

Here we discuss three important limitations of the KELT Variability Catalog in its current form, and discuss possible future directions to address these limitations. The first, is the use of heuristic methods to identify variable objects, the second is the non-detection of most detached eclipsing binaries, and the third is the likelihood of faint contaminants in the KELT photometry.

The selection criteria used in this work, clearly demonstrate the difficulties and current limitations of objectively identifying variable stars in large photometric data sets. While our metrics are based on the reasonable assumption that variability will inflate the dispersion of the light curve, the distributions of each metric are clearly non-Gaussian (see Figure 3). This limits the interpretation of stars which deviate from the main population using typical sigma based cutoffs. While we increased the number of metrics in an attempt to alleviate this tension, increasing the number of metrics used for comparison can ultimately increase the likelihood a star may appear variable due to random sampling error. One way to resolve this issue would be through the use of a neural-net classification. However, there is a current lack of variability training sets available which can properly compensate for the varieties of detector red-noise found in ground based surveys (Pashchenko et al. 2017). Additionally, variable classification is badly imbalanced (there are many more “constant” stars than variable objects in a given data set) which complicates using machine learning techniques. The primary reason we have released the data set through *Filtergraph*, is to provide the astronomical community with a tool for studying and creating a variability training set useful for future study and to allow users to impose their own selection metrics or data cleaning methods.

The periodicity search methods that we have used in this work—Lomb-Scargle based—are not optimized for detection of eclipsing binaries (EBs), especially detached EBs. We expect that we probably have detected contact

EBs in our periodic sample because those light curves are more approximately sinusoidal in nature, but Lomb-Scargle based period-search methods are not optimized for detached EBs whose light curves are characterized by short-duration, punctuated drops in brightness, and moreover generally involve two eclipses per cycle of different depths. We are planning a focused search for EBs as the subject of a separate KELT paper. Even so, any and all EBs in our light curves—even if not yet recognized as such—do have their general variability properties measured and reported in this paper.

As mentioned in § 2, a KELT pixel is $23''$ on a side. This means many of the detected KELT sources are blended with fainter (or in some cases, brighter) neighbors. That blending can cause astrophysical variability from the target star to be diluted, or the signal from a variable blended neighbor can contaminate the signal from the target star. In this analysis, we match the stars in our variable and rotation catalogs to the TIC using a positional match between the 2MASS catalog (Skrutskie et al. 2006) and the base KELT catalog, selecting the nearest 2MASS object within $0.3'$ of the KELT source. Because both the TIC and 2MASS have higher spatial resolution than the KELT catalog, multiple TIC point sources will typically occupy any given KELT pixel. Therefore, future analysis of the KELT data set, when matched to other, higher spatial resolution photometric catalogs, may benefit from an updated matching scheme which incorporates position, magnitude and color rather than position alone.

6. SUMMARY

We have presented an in depth search for variable and periodic sources in the KELT data set. We identify 52,741 stars with large-amplitude modulations and/or periodic signals likely due to stellar variability using 4 variability metrics (rms , Δ_{90} , Welch-Stetson J and L) and by forcing each period to meet 4 requirements. Of these variable objects, 18,907 have all quality flags set to 0, meaning they are unlikely to be contaminated by any detector systematics, aliasing or crowding/blending due KELT’s wide FoV.

We have matched our catalog to the TIC and VSX. Additionally, we identified candidate rotation periods for 62,229 high priority dwarfs, which may be observed with the mission’s 2-minute cadence. Finally, we provided variability upper limits for all other ~ 4 million sources observed by KELT and in the TIC.

The full variable catalog has been uploaded to the *Filtergraph* data visualization portal at the URL https://filtergraph.com/kelt_vars. The portal can be used to access the variability and periodicity information described in § 3.1 and § 3.2, stellar parameters obtained by the cross-matches listed in § 4.3 and § 4.4, and a light curve figure for each variable star for visual inspection. This portal is meant to be a living database and will be updated for new TIC versions, updated KELT observations and any improvements to the variability selection metrics. Basic python code used to calculate the variability and periodicity metrics is available through the GITHUB URL https://github.com/ryanoelkers/var_tests.

We thank the anonymous referee and statistics consul-

tant for their comments and suggestions which greatly improved the quality of this manuscript. Work performed by J.E.R. was supported by the Harvard Future Faculty Leaders Postdoctoral fellowship. This work has made extensive use of the Filtergraph data visualization service (Burger et al. 2013) at <http://www.filtergraph.vanderbilt.edu>. This research has made use of the VizieR catalogue access tool, CDS, Strasbourg, France. This work has made use of the TIC and CTL, through the TESS Science Office’s target selection working group (architects K. Stassun, J. Pepper, N. De Lee, M. Paegert, R. Oelkers). The *Filtergraph* data portal system is trademarked by Vanderbilt University.

REFERENCES

- Alard, C. 2000, *A&AS*, 144, 363
 Alard, C., & Lupton, R. H. 1998, *ApJ*, 503, 325
 Ansdell, M., Oelkers, R. J., Rodriguez, J. E., et al. 2017, *ArXiv e-prints*, arXiv:1707.07313
 Bakos, G., Noyes, R. W., Kovács, G., et al. 2004, *PASP*, 116, 266
 Bakos, G. Á., Csabry, Z., Penev, K., et al. 2013, *PASP*, 125, 154
 Basri, G., Walkowicz, L. M., Batalha, N., et al. 2011, *AJ*, 141, 20
 Bastien, F. A., Stassun, K. G., Basri, G., & Pepper, J. 2013, *Nature*, 500, 427
 Beatty, T. G., Pepper, J., Siverd, R. J., et al. 2012, *ApJ*, 756, L39
 Bieryla, A., Collins, K., Beatty, T. G., et al. 2015, *AJ*, 150, 12
 Blažko, S. 1907, *Astronomische Nachrichten*, 175, 325
 Borucki, W. J., Koch, D., Basri, G., et al. 2010, *Science*, 327, 977
 Boyajian, T. S., LaCourse, D. M., Rappaport, S. A., et al. 2016, *MNRAS*, 457, 3988
 Burger, D., Stassun, K. G., Pepper, J. A., et al. 2013, in *Astronomical Society of the Pacific Conference Series*, Vol. 475, *Astronomical Data Analysis Software and Systems XXII*, ed. D. N. Friedel, 399
 Cargile, P. A., James, D. J., Pepper, J., et al. 2014, *ApJ*, 782, 29
 Ciardi, D. R., & Howell, S. B. 2017, in *American Astronomical Society Meeting Abstracts*, Vol. 229, *American Astronomical Society Meeting Abstracts*, 104.04
 Collins, K. A., Eastman, J. D., Beatty, T. G., et al. 2014, *AJ*, 147, 39
 Díaz, M. C., Beroiz, M., Peñuela, T., et al. 2016, *ApJ*, 828, L16
 Eastman, J. D., Beatty, T. G., Siverd, R. J., et al. 2016, *AJ*, 151, 45
 Fulton, B. J., Collins, K. A., Gaudi, B. S., et al. 2015, *ApJ*, 810, 30
 Gaudi, B. S., Stassun, K. G., Collins, K. A., et al. 2017, *Nature*, advance online publication, letter
 Hartman, J. D., Stanek, K. Z., Gaudi, B. S., Holman, M. J., & McLeod, B. A. 2005, *AJ*, 130, 2241
 Hawley, S. L., Davenport, J. R. A., Kowalski, A. F., et al. 2014, *ApJ*, 797, 121
 Henderson, C. B., & Stassun, K. G. 2012, *ApJ*, 747, 51
 Ivezić, Z., Tyson, J. A., Abel, B., et al. 2008, *ArXiv e-prints*, arXiv:0805.2366
 Jurcsik, J., Sódor, Á., Szeidl, B., et al. 2009, *MNRAS*, 400, 1006
 Kinemuchi, K., Smith, H. A., Woźniak, P. R., McKay, T. A., & ROTSE Collaboration. 2006, *AJ*, 132, 1202
 Kovács, G., Bakos, G., & Noyes, R. W. 2005, *MNRAS*, 356, 557
 Kowalski, A. F., Hawley, S. L., Hilton, E. J., et al. 2009, *AJ*, 138, 633
 Kraft, R. P. 1967, *ApJ*, 150, 551
 Kuhn, R. B., Rodriguez, J. E., Collins, K. A., et al. 2016, *MNRAS*, 459, 4281
 Labadie-Bartz, J., Pepper, J., McSwain, M. V., et al. 2017, *AJ*, 153, 252
 Law, N. M., Carlberg, R., Salbi, P., et al. 2013, *AJ*, 145, 58
 Liang, E.-S., Wang, S., Zhou, J.-L., et al. 2016, *AJ*, 152, 168
 Lomb, N. R. 1976, *Ap&SS*, 39, 447
 Long, J. P., Chi, E. C., & Baraniuk, R. G. 2016, *Ann. Appl. Stat.*, 10, 165
 Lund, M. B., Rodriguez, J. E., Zhou, G., et al. 2017, *AJ*, 154, 194
 McLeod, K. K., Rodriguez, J. E., Oelkers, R. J., et al. 2017, *AJ*, 153, 263
 Oberst, T. E., Rodriguez, J. E., Colón, K. D., et al. 2017, *AJ*, 153, 97
 Oelkers, R. J., Macri, L. M., Marshall, J. L., et al. 2016a, *AJ*, 152, 75
 Oelkers, R. J., Macri, L. M., Wang, L., et al. 2015, *AJ*, 149, 50
 —. 2016b, *AJ*, 151, 166
 Pashchenko, I. N., Sokolovsky, K. V., & Gavras, P. 2017, *ArXiv e-prints*, arXiv:1710.07290
 Pepper, J., Kuhn, R. B., Siverd, R., James, D., & Stassun, K. 2012, *PASP*, 124, 230
 Pepper, J., Pogge, R. W., DePoy, D. L., et al. 2007, *PASP*, 119, 923
 Pepper, J., Siverd, R. J., Beatty, T. G., et al. 2013, *ApJ*, 773, 64
 Pepper, J., Rodriguez, J. E., Collins, K. A., et al. 2017, *AJ*, 153, 215
 Pietrukowicz, P. 2001, *Acta Astron.*, 51, 247
 Pigulski, A., & Pojmański, G. 2008, *A&A*, 477, 917
 Pilecki, B., Fabrycky, D., & Poleski, R. 2007, *MNRAS*, 378, 757
 Pojmanski, G. 1997, *Acta Astron.*, 47, 467
 —. 2002, *Acta Astron.*, 52, 397
 —. 2003, *Acta Astron.*, 53, 341
 Pojmanski, G., & Maciejewski, G. 2004, *Acta Astron.*, 54, 153
 —. 2005, *Acta Astron.*, 55, 97
 Pojmanski, G., Pilecki, B., & Szczygiel, D. 2005, *Acta Astron.*, 55, 275
 Pollacco, D. L., Skillen, I., Collier Cameron, A., et al. 2006, *PASP*, 118, 1407
 Ricker, G. R., Winn, J. N., Vanderspek, R., et al. 2014, in *Proc. SPIE*, Vol. 9143, *Space Telescopes and Instrumentation 2014: Optical, Infrared, and Millimeter Wave*, 914320
 Rodriguez, J. E., Pepper, J., & Stassun, K. G. 2016a, in *IAU Symposium*, Vol. 314, *Young Stars & Planets Near the Sun*, ed. J. H. Kastner, B. Stelzer, & S. A. Metchev, 167–170
 Rodriguez, J. E., Pepper, J., Stassun, K. G., et al. 2013, *AJ*, 146, 112
 —. 2015, *AJ*, 150, 32
 Rodriguez, J. E., Stassun, K. G., Lund, M. B., et al. 2016b, *AJ*, 151, 123
 Rodriguez, J. E., Colón, K. D., Stassun, K. G., et al. 2016c, *AJ*, 151, 138
 Rodriguez, J. E., Ansdell, M., Oelkers, R. J., et al. 2017a, *ApJ*, 848, 97
 Rodriguez, J. E., Zhou, G., Cargile, P. A., et al. 2017b, *ApJ*, 836, 209
 Samus’, N. N., Kazarovets, E. V., Durlevich, O. V., Kireeva, N. N., & Pastukhova, E. N. 2017, *Astronomy Reports*, 61, 80
 Scargle, J. D. 1982, *ApJ*, 263, 835
 Siverd, R. J., Goobar, A., Stassun, K. G., & Pepper, J. 2015, *ApJ*, 799, 105
 Siverd, R. J., Beatty, T. G., Pepper, J., et al. 2012, *ApJ*, 761, 123
 Siverd, R. J., Collins, K. A., Zhou, G., et al. 2017, *ArXiv e-prints*, arXiv:1709.07010
 Skrutskie, M. F., Cutri, R. M., Stiening, R., et al. 2006, *AJ*, 131, 1163
 Stassun, K. G., Mathieu, R. D., Mazeh, T., & Vrba, F. J. 1999, *AJ*, 117, 2941
 Stassun, K. G., Oelkers, R. J., Pepper, J., et al. 2017, *ArXiv e-prints*, arXiv:1706.00495
 Stetson, P. B. 1987, *PASP*, 99, 191
 —. 1996, *PASP*, 108, 851
 Stevens, D. J., Collins, K. A., Gaudi, B. S., et al. 2017, *AJ*, 153, 178
 Szczygiel, D. M., Pojmański, G., & Pilecki, B. 2009, *Acta Astron.*, 59, 137
 Tayar, J., Ceillier, T., García-Hernández, D. A., et al. 2015, *ApJ*, 807, 82
 Temple, L. Y., Hellier, C., Albrow, M. D., et al. 2017, *ArXiv e-prints*, arXiv:1704.07771
 Udalski, A., Szymanski, M., Stanek, K. Z., et al. 1994, *Acta Astron.*, 44, 165
 van Saders, J. L., & Pinsonneault, M. H. 2013, *ApJ*, 776, 67
 VanderPlas, J. T. 2017, *ArXiv e-prints*, arXiv:1703.09824

- Wang, L., Macri, L. M., Krisciunas, K., et al. 2011, *AJ*, 142, 155
- Wang, L., Macri, L. M., Wang, L., et al. 2013, *AJ*, 146, 139
- Watson, C. L. 2006, *Journal of the American Association of Variable Star Observers (JAAVSO)*, 35, 318
- Woźniak, P. R., Williams, S. J., Vestrand, W. T., & Gupta, V. 2004a, *AJ*, 128, 2965
- Woźniak, P. R., Vestrand, W. T., Akerlof, C. W., et al. 2004b, *AJ*, 127, 2436
- Young, A. T. 1967, *AJ*, 72, 747
- Zhou, G., Rodriguez, J. E., Collins, K. A., et al. 2016, *AJ*, 152, 136

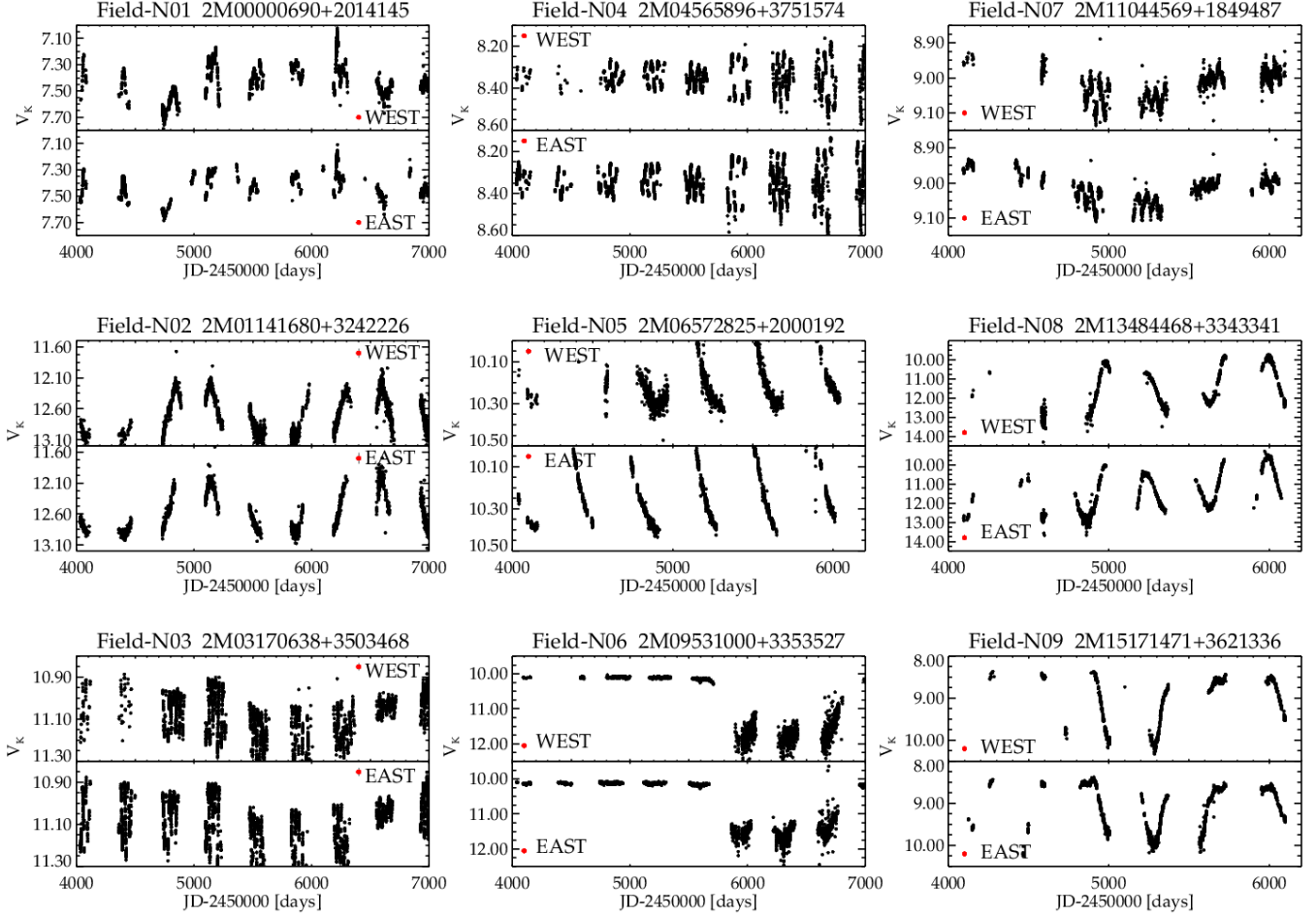


FIG. 9.— 9 representative light curves for objects identified using the variability metrics described in § 3.1 from 9 northern fields in the KELT data set. Each sub-panel shows the light curves from both the W (top) and E (bottom) orientations. The light curves have been split by field orientation to emphasize the star is displaying similar variability in *both* field orientations. Typical photometric errors are shown next to the field orientation as red points.

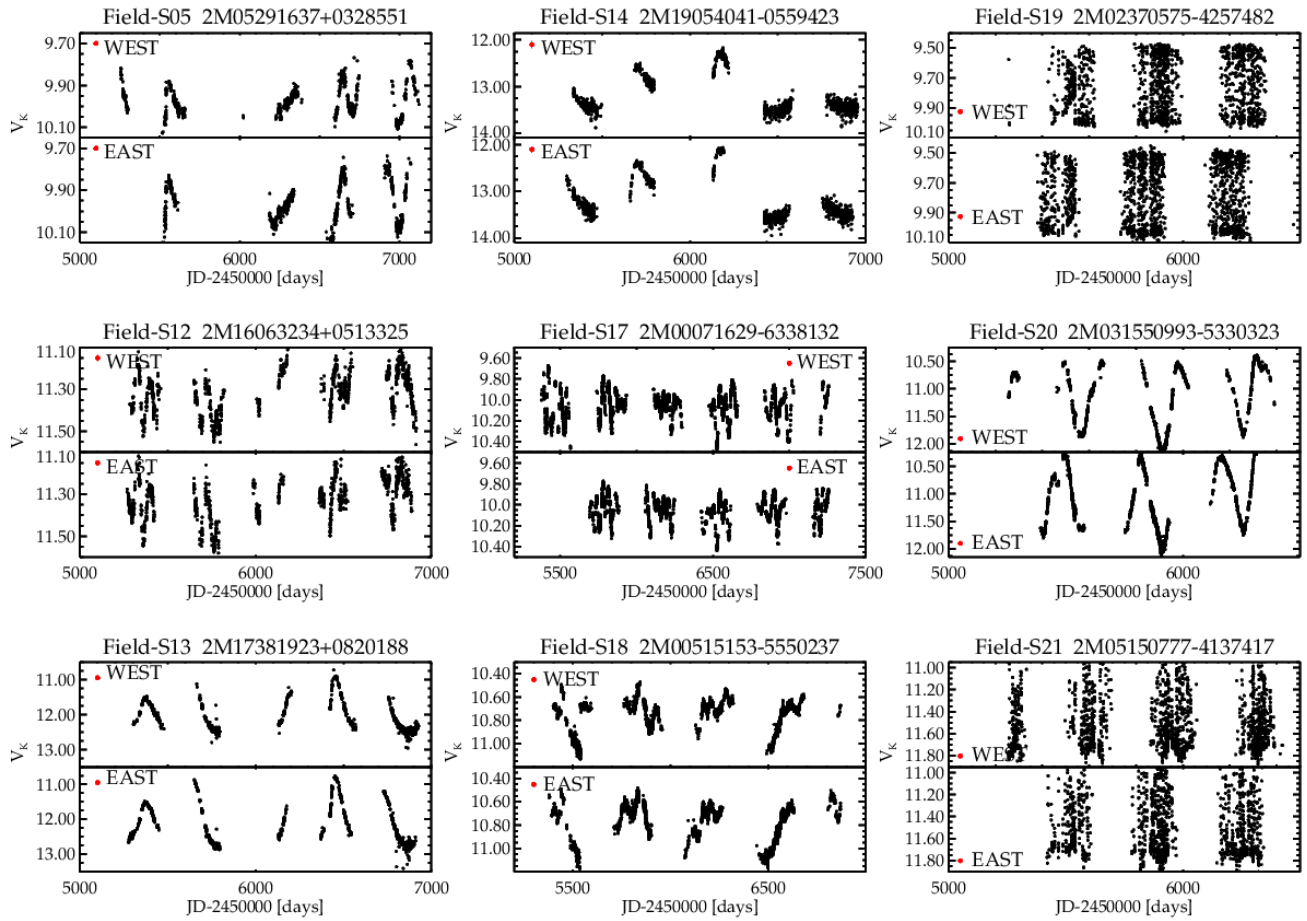


FIG. 10.— Same as Figure 9 but for 9 southern KELT fields.

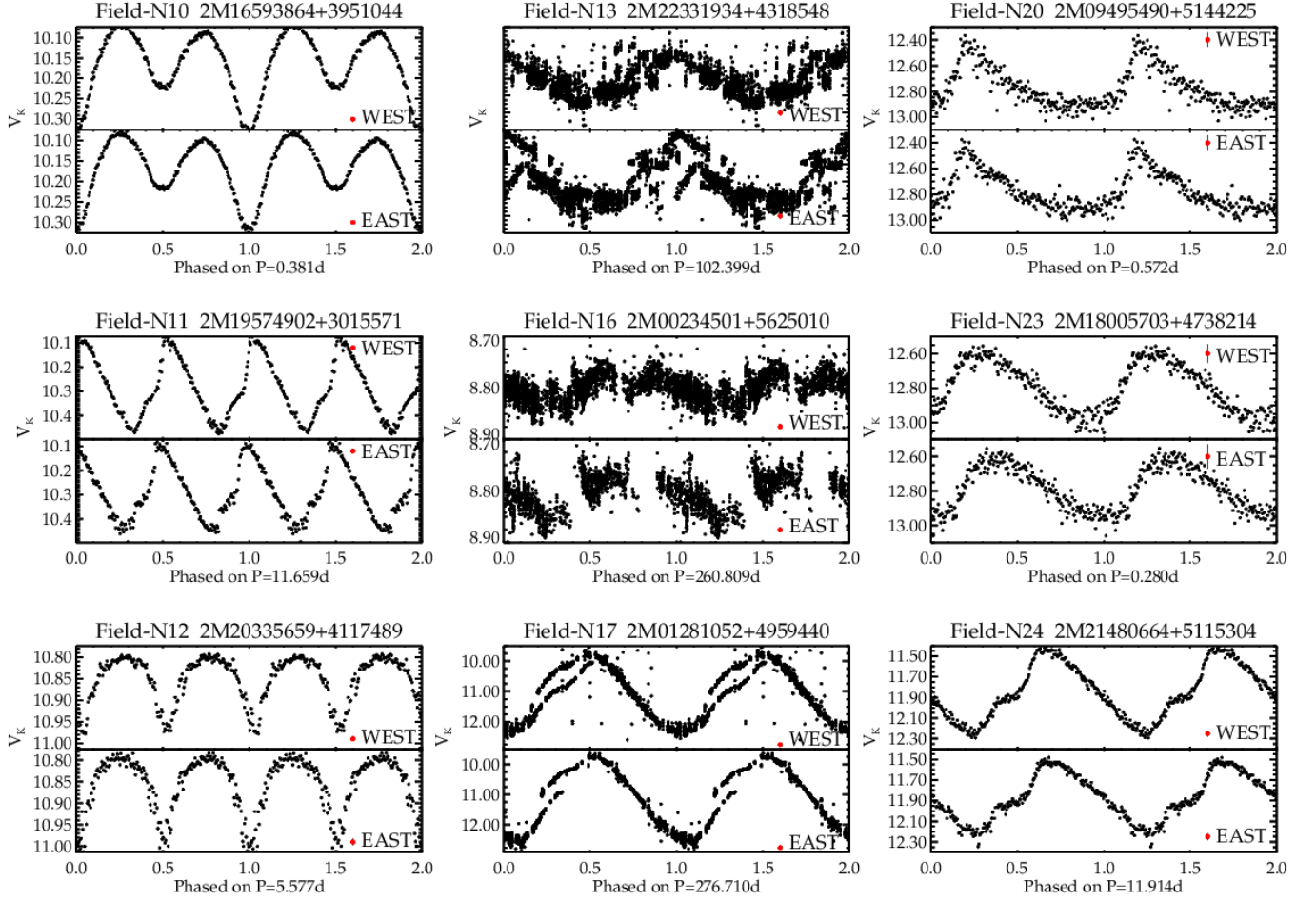


FIG. 11.— 9 representative light curves of objects identified using the periodicity requirements described in § 3.2 from 9 northern fields in the KELT data set. Each sub-panel shows the light curves from both the W (top) and E (bottom) orientations. The light curves have been split by field orientation to emphasize the star is displaying similar periodicity in *both* field orientations. Typical photometric errors are shown next to the field orientation as red points. The light curves have been phased on the period shown below the x-axis and plotted twice for clarity. Light curves shown for stars with periods $P < 100$ days were binned into 200 phase bins after phase folding. Light curves shown for stars with periods $P > 100$ days were not binned after phase folding.

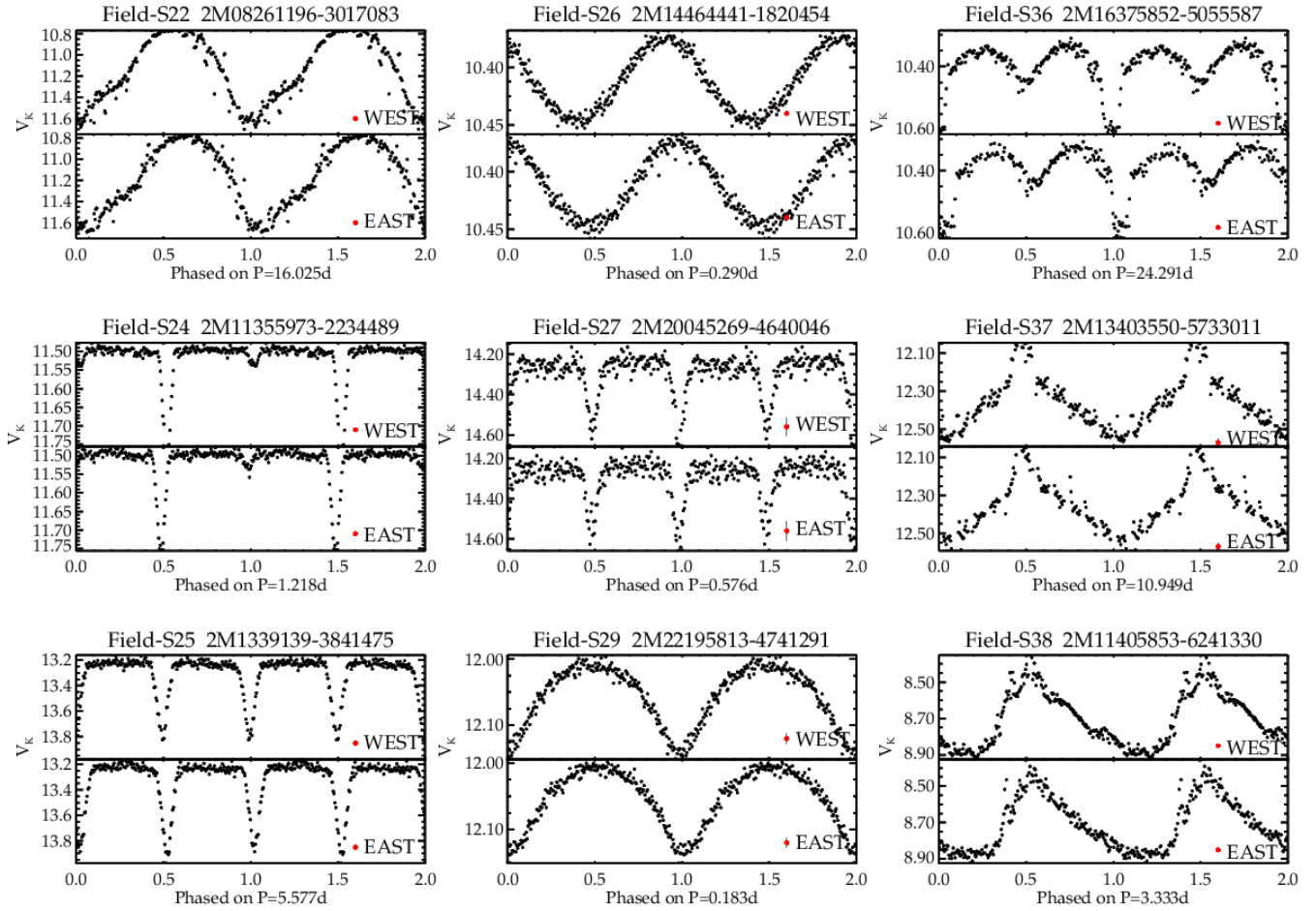


FIG. 12.— Same as Figure 11 but for 9 southern KELT fields.

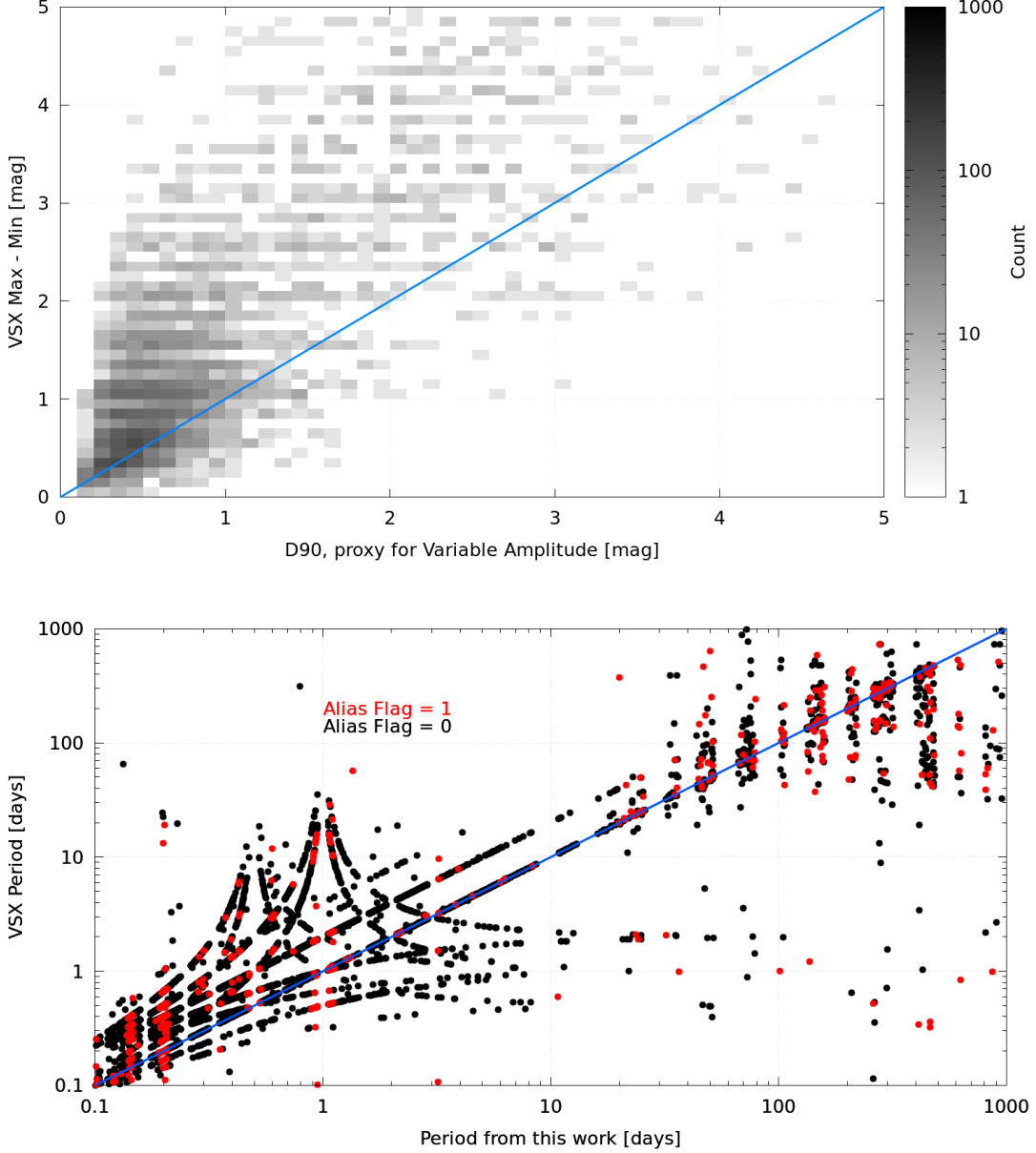


FIG. 13.— *Top*: Comparisons of 6,000 stars which passed the variable metrics described in § 3.1 and are also identified in the VSX database. Here we use the absolute difference between the VSX reported maximum and minimum magnitude to estimate the amplitude in the VSX and use the Δ_{90} metric to estimate the amplitude in our catalog. While ~ 700 stars have show similar amplitude, in general the VSX reports a larger change in magnitude than our catalog. *Bottom*: Comparisons of the 6,333 stars, with periods between 0.1 and 1000 d, identified in the VSX database (y-axis) and this work (x-axis). The 757 red points denote stars with their alias flag set to 1, meaning they may be affected by strong detector aliasing (see § 3.3). The 5,576 black points denote stars which have their alias flag set to 0, meaning they are unlikely to be affected by strong detector aliasing. The blue line denotes a 1-1 relationship. 3,564 stars show a period within the first 2 (sub-)harmonics of the VSX period. Many periods recovered by the VSX or this work also show parabolic signatures, likely describing higher order (sub-)harmonics recovery as seen in Long et al. (2016); VanderPlas (2017).

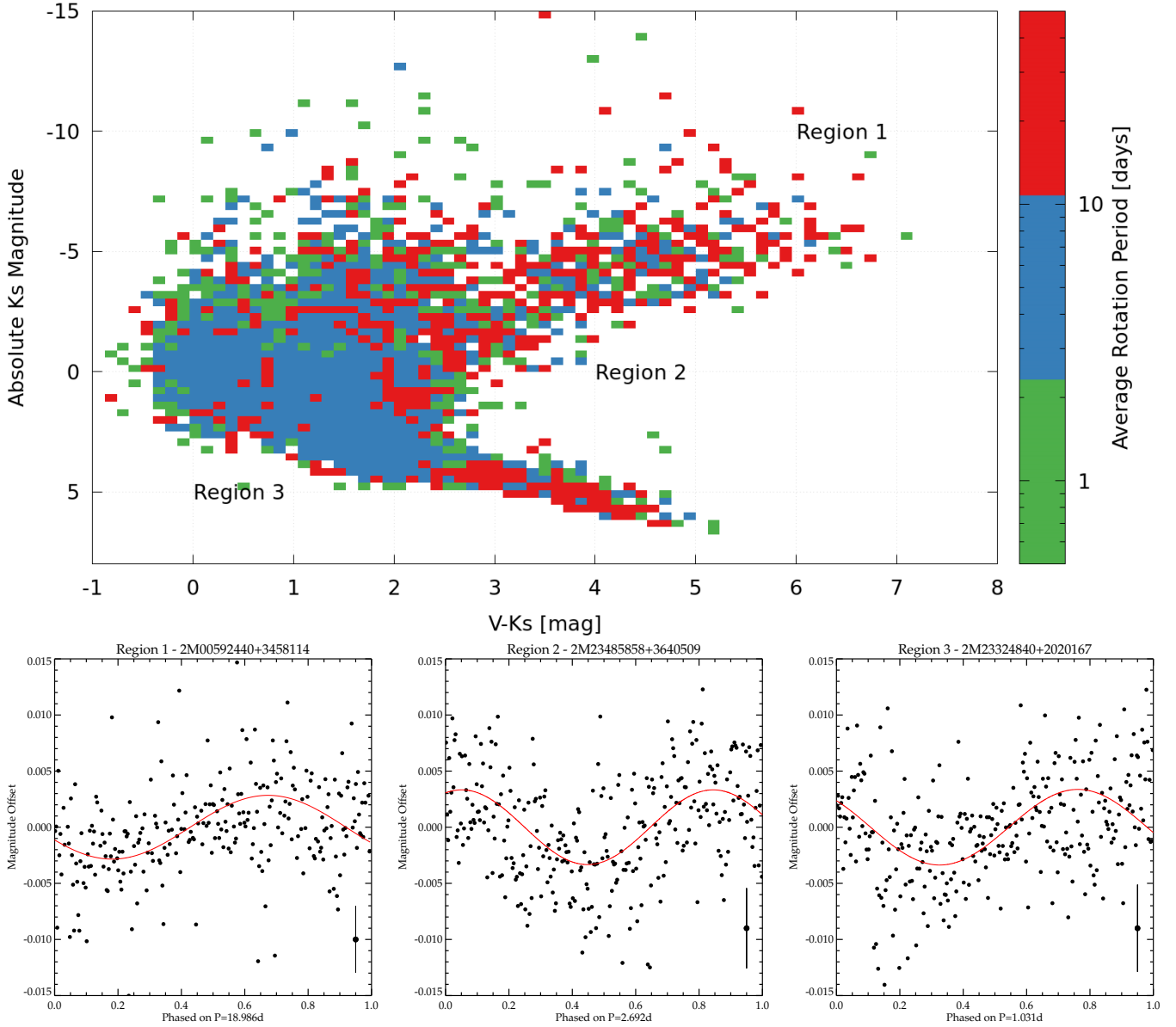


FIG. 14.— *Top*: A heatmap, colored by average period, of an H-R diagram of KELT stars with valid rotation periods less than 50 days and parallaxes provided by the TIC from the analysis described in § 4.3.2. The V magnitude in this figure is the Johnson V magnitude reported in the TIC, and not V_K . Stars with the longest periods are found along the giant branch, as is expected. The figure has been broken into 3 regions. Region 1: the giant branch, Region 2: sub-giant stars, Region 3: dwarf stars. *Bottom*: 3 representative light curves of periodic stars, one from each of the 3 regions in the top panel. The solid red lines are the best fit sine curve to each phased light curve. Each light curve has been phased on the period recovered for the star and binned into 400 data points. Representative error bars can be found at the bottom right of each panel. The stars have had their E and W orientation light curves combined and de-trended for these figures and the analysis.

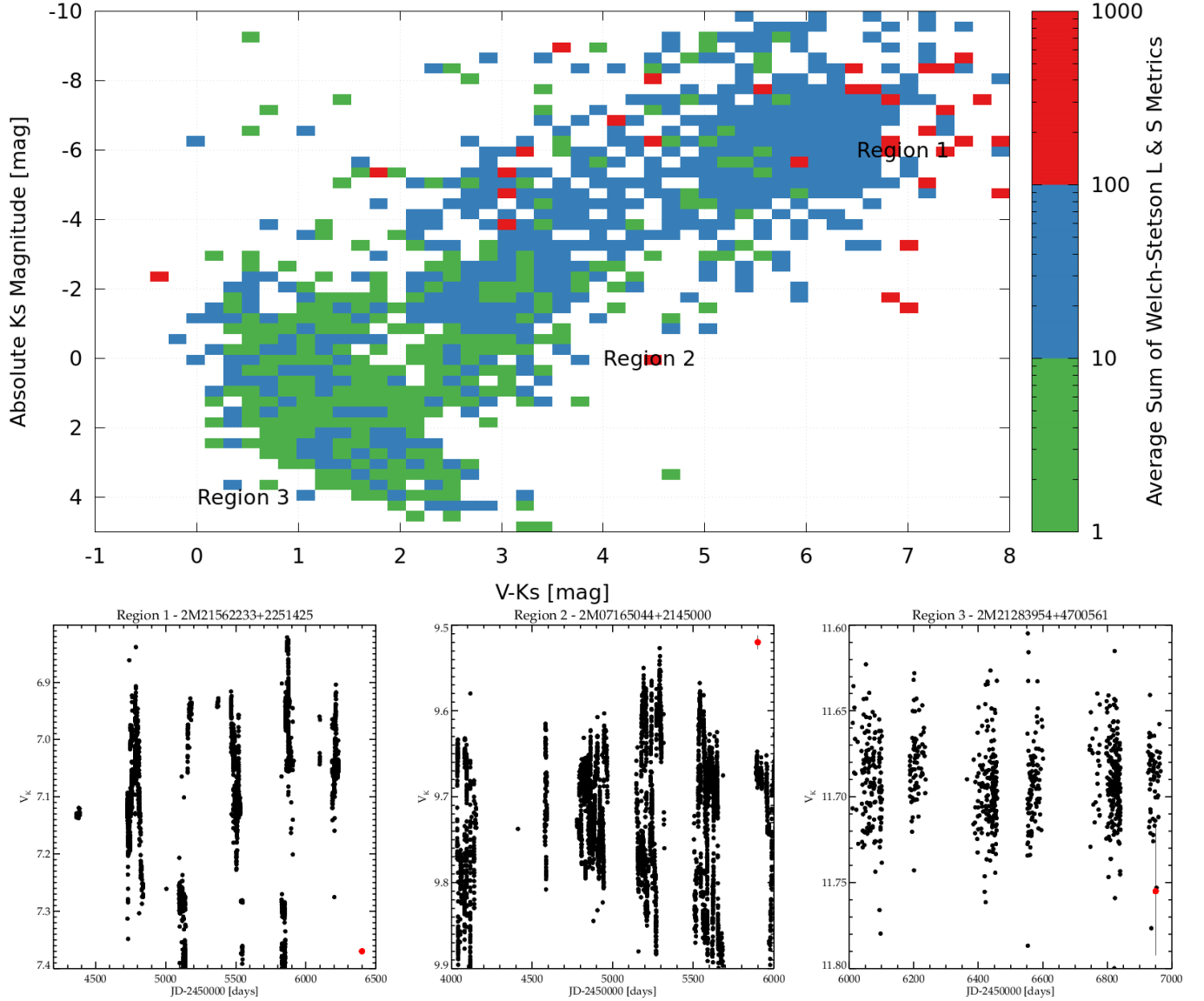


FIG. 15.— *Top*: A heatmap, colored by the sum of the Welch-Stetson J and L metrics, of an H-R diagram for stars in the KELT variable data set with valid parallaxes provided by the TIC. The V magnitude in this figure is the Johnson V magnitude reported in the TIC, and not V_K . *Bottom*: 3 representative light curves of variable stars in the top panel, one of each of the 3 regions. Each light curve has been binned into 30 minute intervals. Representative error bars can be found at the bottom right of each panel. The stars have had their E and W orientation light curves combined for these figures.

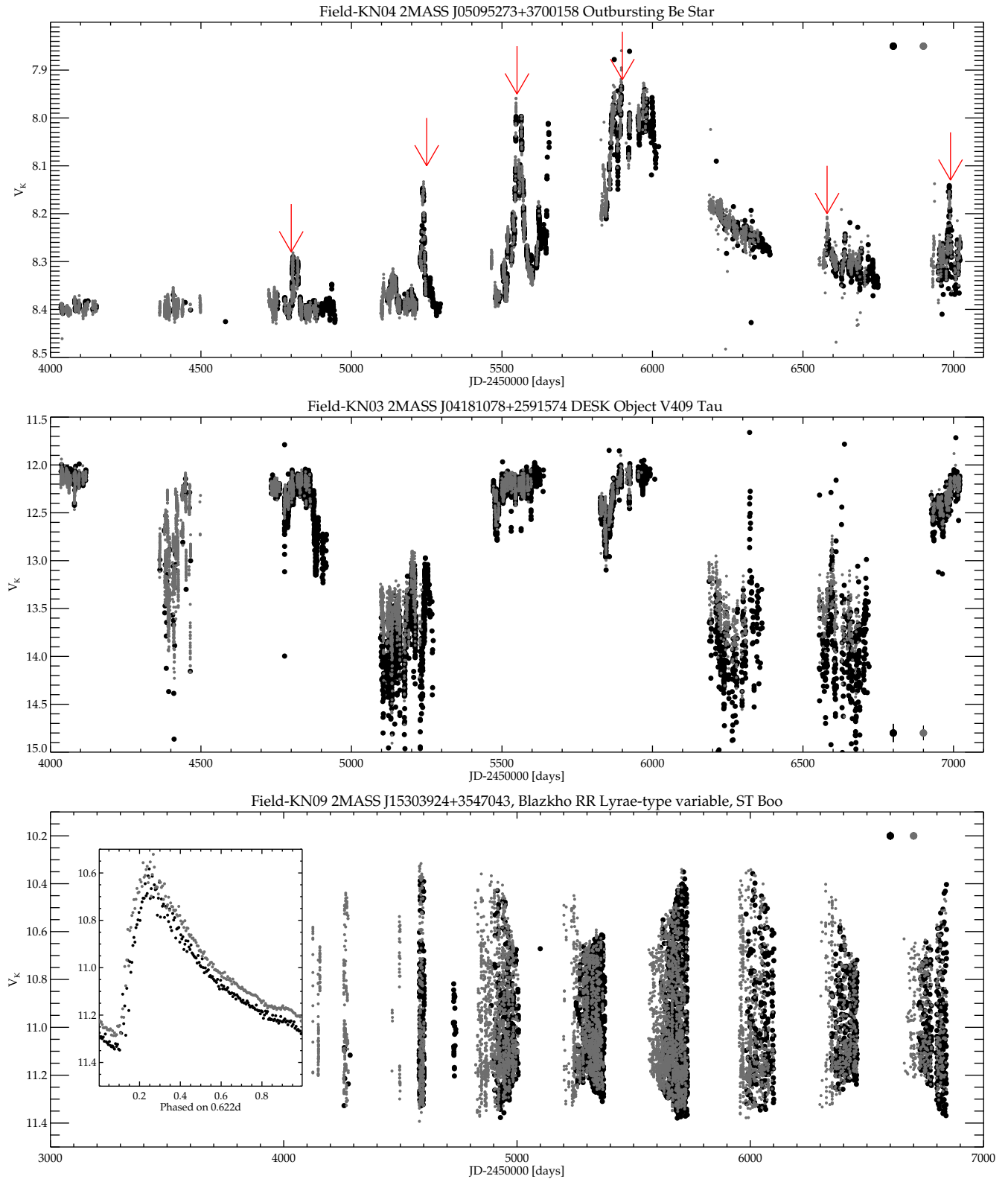


FIG. 16.— Three KELT variables, two of which were previously identified in other KELT variable surveys, with observed long term variation aided by the long KELT baseline (> 5 yr). The grey points are from the E orientation and the the black points are from the W orientation in each panel. Typical photometric errors can be seen at the top right of the first and third panels and at the bottom right of the second panel. *Top*: 2MASS J05095273+3700158 candidate Be star with regular outbursts (marked with red arrows) originally identified in Labadie-Bartz et al. (2017). *Middle*: 2MASS J04181078+2591574, also known as V409 Tau, is a young star regularly eclipsed by a protoplanetary disk first identified in Rodriguez et al. (2015). *Bottom*: 2MASS J15303924+3547043 an RR Lyrae-type variable, ST Boo, with Blazkho effect modulation. The phased light curve with a period of 0.622 days is shown in the inset of the bottom panel.

TABLE 1
 KELT FIELDS INVESTIGATED FOR VARIABLES

Field Name	North/South	Approximate α [hh:mm.m]	Field Center δ [dd:mm]	Julian Date Start	Julian Date End	Star Count	Variables Identified
N01	North	00:06.0	+31:40	2454034	2457016	66592	653
N02	North	02:01.8	+31:40	2454034	2457018	85828	363
N03	North	03:58.2	+31:40	2454034	2457020	98259	722
N04	North	05:54.0	+31:40	2454035	2457022	172816	1875
N05	North	07:50.4	+31:40	2454035	2456039	95805	749
N06	North	09:46.2	+31:40	2454035	2457022	49412	321
N07	North	11:42.6	+31:40	2454093	2456100	23254	223
N08	North	13:38.4	+31:40	2454094	2456100	38660	272
N09	North	15:34.8	+31:40	2454124	2456840	49723	386
N10	North	17:30.6	+31:40	2454154	2456457	66233	1198
N11	North	19:27.0	+31:40	2454250	2456986	165927	2621
N12	North	21:22.8	+31:40	2454259	2456457	162204	2402
N13	North	23:19.2	+31:40	2454034	2456100	56788	766
N16	North	00:03.0	+57:00	2456068	2457022	145870	1914
N17	North	02:43.2	+57:00	2455973	2457021	139849	434
N20	North	10:43.2	+57:00	2455976	2456455	57248	259
N23	North	18:43.2	+57:00	2455978	2456991	134183	885
N24	North	21:23.4	+57:00	2456009	2457021	131756	2418
S05	South	06:07.8	+03:00	2455256	2457122	169498	1718
S12	South	16:52.2	+03:00	2455268	2456914	145044	1143
S13	South	18:24.0	+03:00	2455275	2457101	163723	2824
S14	South	19:55.8	+03:00	2455298	2456954	215161	4578
S17	South	00:00.0	-53:00	2455378	2457256	39670	513
S18	South	01:31.8	-53:00	2455378	2456870	44482	491
S19	South	03:04.2	-53:00	2455256	2456471	46246	243
S20	South	04:36.0	-53:00	2455256	2456390	68403	512
S21	South	06:07.8	-53:00	2455256	2456769	97360	1126
S22	South	09:12.0	-20:00	2455256	2457027	154456	1644
S23	South	10:43.8	-20:00	2455268	2456848	92255	247
S24	South	12:16.2	-30:00	2455268	2456510	102385	806
S25	South	13:48.0	-30:00	2455268	2457056	102303	1149
S26	South	15:19.8	-20:00	2455268	2457223	120235	1126
S27	South	19:55.8	-53:00	2455268	2457223	111056	1498
S29	South	23:00.0	-53:00	2455268	2457223	51019	672
S32	South	00:04.1	-29:50	2455803	2456871	66383	376
S34	South	08:16.0	-54:00	2455200	2456822	178687	2373
S36	South	17:24.0	-53:00	2456428	2457309	219968	5968
S37	South	15:07.2	-53:00	2456541	2457277	132493	2330
S38	South	12:50.4	-53:00	2456647	2457385	208826	2982

NOTE. — *: The coordinates of each field are an approximation of each field center. The star counts and Julian Dates of the fields represent the data in this work and may vary for future and alternate reductions.

TABLE 2
ASTROMETRIC INFORMATION FOR KELT VARIABLES

2MASS ID	TIC ID	Coordinates		Proper Motions [mas/yr]		Parallax π [mas]
		α [hh:mm:ss.s]	δ [dd:mm:ss]	μ_α	μ_δ	
J00000082+2558023	407307771	00:00:00.8	25:58:02	-1.90 ± 2.20	3.80 ± 2.20	—
J00000690+2014145	380152855	00:00:06.9	20:14:15	-11.00 ± 1.30	-17.50 ± 1.40	—
J00000657+2553112	117927634	00:00:06.6	25:53:11	13.20 ± 2.20	-10.00 ± 2.20	5.1700 ± 1.9500
J00001686+2636285	117927399	00:00:16.9	26:36:29	1.60 ± 0.80	-2.40 ± 1.20	—
J00001766+2555323	117927619	00:00:17.7	25:55:32	-19.60 ± 2.30	13.40 ± 2.80	—
J00003558+2639495	117929062	00:00:35.6	26:39:50	5.00 ± 1.60	-18.70 ± 1.80	—
J00010148+1937371	380157330	00:01:01.5	19:37:37	-29.60 ± 1.80	-14.50 ± 2.40	—
J00010244+3830145	432552443	00:01:02.4	38:30:15	1.50 ± 5.70	-2.20 ± 5.40	—
J00012877+3147256	83957575	00:01:28.8	31:47:26	-10.80 ± 4.00	-6.40 ± 4.00	—
—	—	00:03:09.4	44:09:60	—	—	—
J00032115+4047086	194140962	00:03:21.2	40:47:09	-4.20 ± 2.80	-1.10 ± 2.70	—
J00032141+3831068	194142243	00:03:21.4	38:31:07	-5.10 ± 3.10	-8.90 ± 2.10	—
J00032799+3047161	396382654	00:03:28.0	30:47:16	4.50 ± 2.30	1.20 ± 2.60	—
J00033731+3508290	396392898	00:03:37.3	35:08:29	4.39 ± 1.72	0.85 ± 0.98	1.2514 ± 0.6556
J00034949+3153160	396383077	00:03:49.5	31:53:16	0.40 ± 3.80	8.50 ± 2.50	—
J00035473+4006068	194145862	00:03:54.7	40:06:07	17.06 ± 0.79	0.67 ± 1.27	2.8781 ± 0.4251
J00040465+3814184	194144802	00:04:04.7	38:14:18	-7.20 ± 1.50	-0.80 ± 1.90	—
J00040750+1946581	238304364	00:04:07.5	19:46:58	-1.70 ± 0.70	-18.70 ± 1.00	—
J00040792+4010437	194145915	00:04:07.9	40:10:44	-2.17 ± 2.44	-6.73 ± 2.29	0.7748 ± 0.8288
J00040905+3418094	396393959	00:04:09.1	34:18:09	-3.80 ± 1.90	-5.50 ± 2.30	—

NOTE. — *: This is only a part of the full table to be released online. The most up-to-date version of this table, including updates from new versions of the TIC, additional KELT observations or improved selection metrics is available for download at the *Filtergraph* portal [https://filtergraph.com/kelt\\$_\\$vars](https://filtergraph.com/kelt$_$vars).

TABLE 3
MAGNITUDE INFORMATION FOR KELT VARIABLES

2MASS ID	Magnitudes													
	V_K	T	B	V	g	r	i	J	H	K_S	W_1	W_2	W_3	W_4
J00000082+2558023	11.056	10.710	11.673	11.204	11.416	11.099	11.277	10.249	10.047	10.021	9.970	9.998	10.110	8.168
J00000690+2014145	7.434	6.361	—	—	—	—	—	4.026	3.079	2.562	0.652	0.964	2.072	1.579
J00000657+2553112	7.796	5.520	11.528	10.377	11.310	99.999	99.999	2.225	1.317	0.915	—	—	—	—
J00001686+2636285	10.273	9.193	13.258	11.712	12.405	11.097	99.999	7.346	6.544	6.183	5.662	5.090	3.988	3.106
J00001766+2555323	11.495	12.661	14.569	13.577	14.074	13.224	13.317	11.823	11.399	11.269	11.189	11.301	11.119	8.615
J00003558+2639495	13.081	12.819	13.657	13.337	13.449	13.253	13.123	12.344	12.224	12.116	11.963	11.959	11.692	9.003
J00010148+1937371	12.704	12.426	13.682	13.050	13.349	12.869	12.734	11.852	11.547	11.540	11.458	11.480	11.599	8.966
J00010244+3830145	9.021	6.669	12.918	11.157	12.167	10.246	7.783	3.542	2.630	2.083	-0.506	0.077	0.737	0.229
J00012877+3147256	9.544	8.024	12.996	11.401	12.147	10.604	8.511	5.719	4.796	4.486	4.238	3.902	3.645	3.011
—	11.062	—	—	—	—	—	—	—	—	—	—	—	—	—
J00032115+4047086	9.318	7.573	13.048	11.282	12.260	10.412	7.564	4.899	3.826	3.344	3.224	2.023	2.225	1.489
J00032141+3831068	12.434	11.687	13.881	12.736	13.280	12.363	11.982	10.697	10.119	9.952	9.870	9.925	9.771	8.969
J00032799+3047161	13.314	12.744	14.024	13.379	13.645	13.201	13.055	12.167	11.950	11.859	11.784	11.792	11.579	8.989
J00033731+3508290	9.686	8.095	12.736	11.129	11.849	10.437	8.580	5.985	5.134	4.791	4.651	4.555	4.480	4.212
J00034949+3153160	12.572	11.972	13.112	12.598	12.799	12.438	12.210	11.402	11.179	11.100	11.121	11.145	11.046	8.598
J00035473+4006068	11.788	11.461	12.815	12.144	12.441	11.955	11.759	10.836	10.536	10.483	10.452	10.488	10.455	8.989
J00040465+3814184	12.470	11.797	13.241	12.532	12.858	12.324	12.125	11.071	10.691	10.568	10.588	10.603	10.592	8.750
J00040750+1946581	12.498	11.876	13.006	12.418	12.678	12.255	12.068	11.312	11.009	10.936	10.850	10.866	10.786	8.574
J00040792+4010437	10.650	10.158	12.208	11.128	11.643	10.792	10.421	9.223	8.643	8.518	8.422	8.526	8.418	8.568
J00040905+3418094	10.759	9.047	13.903	12.258	13.007	11.538	9.572	6.842	5.967	5.637	5.557	5.476	5.224	4.962

NOTE. — *: This is only a part of the full table to be released online. The most up-to-date version of this table, including updates from new versions of the TIC, additional KELT observations or improved selection metrics is available for download at the *Filtergraph* portal [https://filtergraph.com/kelt\\$_\\$vars](https://filtergraph.com/kelt$_$vars).

TABLE 4
VARIABILITY INFORMATION FOR KELT VARIABLES

2MASS ID	V_K	rms	Δ_{90}	J_S	L_S	Period [d]	Power	A_P	Variable	Variability Periodic	Multi-P	Alias	Blend	Quality Prox.	Quality Points	Flags	Edge	Single
J0000082+2558023	11.056	0.136	0.424	7.705	5.682	—	0.000	0.000	1	0	0	0	0	0	0	0	0	0
J00000690+2014145	7.434	0.117	0.380	47.588	34.013	—	0.000	0.000	1	0	0	0	0	0	0	0	0	0
J00000657+2553112	7.796	0.615	1.782	277.130	207.578	—	0.000	0.000	1	0	0	0	0	0	0	0	0	0
J00001686+2636285	10.273	0.236	0.820	15.561	10.755	—	0.000	0.000	1	0	0	0	0	0	0	0	0	0
J00001766+2555323	11.495	0.951	3.004	41.226	28.022	—	0.000	0.000	1	0	0	0	0	0	1	0	0	1
J00003558+2639495	13.081	0.217	0.696	1.455	1.041	1.309193	0.526	2.620	1	1	1	0	0	0	0	0	0	1
J00010148+1937371	12.704	0.145	0.440	1.149	0.777	—	0.000	0.000	1	0	0	0	0	0	0	0	1	1
J00010244+3830145	9.021	0.199	0.628	59.084	45.950	—	0.000	0.000	1	0	0	0	0	0	0	0	0	0
J00012877+3147256	9.544	0.158	0.564	22.433	15.298	—	0.000	0.000	1	0	0	0	0	0	0	0	0	0
—	11.062	0.061	0.210	3.221	2.248	—	0.000	0.000	1	0	0	0	0	0	1	0	0	0
J00032115+4047086	9.318	0.170	0.582	34.176	25.764	—	0.000	0.000	1	0	0	0	0	0	0	0	1	0
J00032141+3831068	12.434	0.065	0.212	0.579	0.403	5.929420	0.445	4.650	0	1	1	0	0	0	0	0	0	0
J00032799+3047161	13.314	0.151	0.479	0.691	0.504	0.191503	0.639	3.130	0	1	1	0	0	0	0	0	0	1
J00033731+3508290	9.686	0.068	0.221	9.185	6.720	—	0.000	0.000	1	0	0	0	0	0	0	0	0	0
J00034949+3153160	12.572	0.062	0.200	0.538	0.386	0.219036	0.464	4.570	0	1	1	0	0	0	0	0	0	0
J00035473+4006068	11.788	0.220	0.685	4.456	3.286	—	0.000	0.000	1	0	0	0	0	0	0	0	0	0
J00040465+3814184	12.470	0.097	0.328	0.924	0.614	0.201513	0.455	5.070	0	1	0	0	0	0	0	0	0	0
J00040750+1946581	12.498	0.107	0.338	0.771	0.547	0.208718	0.543	2.650	0	1	1	0	0	0	0	0	1	1
J00040792+4010437	10.650	0.088	0.281	4.960	3.449	316.582275	0.689	7.640	0	1	0	1	0	0	0	0	0	0
J00040905+3418094	10.759	0.117	0.370	7.930	5.661	—	0.000	0.000	1	0	0	0	0	0	0	0	0	0

NOTE. — *: This is only a part of the full table to be released online. The most up-to-date version of this table, including updates from new versions of the TIC, additional KELT observations or improved selection metrics is available for download at the *Filtergraph* portal [https://filtergraph.com/kelt\\$_s\\$vars](https://filtergraph.com/kelt$_s$vars).

TABLE 5
VARIABILITY UPPER LIMITS FOR NON-VARIABLE SOURCES IN THE *TESS* INPUT CATALOG

2MASS ID	TIC-ID	Coordinates		<i>TESS</i> magnitude	<i>rms</i> [mag]		
		α [hh:mm:ss.s]	δ [dd:mm:ss]		30 m	2 hr	1 d
J00414901+2249449	434216066	00:41:49.0	+22:49:45	8.508	0.004	0.003	0.002
J00374969+2441381	25681585	00:37:49.7	+24:41:38	9.988	0.005	0.003	0.003
J00392215+2220369	434210302	00:39:22.1	+22:20:37	8.499	0.005	0.003	0.003
J00414699+2105384	434216506	00:41:47.0	+21:05:38	9.074	0.005	0.004	0.003
J00421622+2156301	434218239	00:42:16.2	+21:56:30	9.058	0.006	0.004	0.004
J00385815+2332576	434209796	00:38:58.1	+23:32:58	8.652	0.005	0.004	0.003
J00433708+2346437	434221734	00:43:37.1	+23:46:44	9.412	0.011	0.009	0.009
J23482160+2755522	129574905	23:48:21.6	+27:55:52	10.189	0.009	0.006	0.006
J00374045+1928004	242841531	00:37:40.5	+19:28:00	13.89	0.009	0.007	0.006
J00432503+2225024	434222066	00:43:25.0	+22:25:02	9.175	0.006	0.004	0.004
J00442011+2221041	434224025	00:44:20.1	+22:21:04	8.23	0.005	0.004	0.004
J00404825+2052182	434213593	00:40:48.3	+20:52:18	9.599	0.008	0.006	0.005
J00371922+2136420	242841747	00:37:19.2	+21:36:42	8.649	0.005	0.003	0.003
J00402308+2346126	434212944	00:40:23.1	+23:46:13	6.943	0.003	0.002	0.002
J00362178+2241415	426961066	00:36:21.8	+22:41:42	9.38	0.006	0.004	0.004
J00384049+2232164	434207237	00:38:40.5	+22:32:16	9.306	0.006	0.004	0.003
J00415149+2348021	434215825	00:41:51.5	+23:48:02	9.34	0.008	0.006	0.005
J00413447+2118025	434216453	00:41:34.5	+21:18:03	8.609	0.042	0.042	0.031
J00444942+2313366	434224552	00:44:49.4	+23:13:37	9.75	0.008	0.006	0.005
J00393851+2021381	434210831	00:39:38.5	+20:21:38	7.789	0.005	0.004	0.003

NOTE. — *: This is only a part of the full table which is available for bulk download at the URL [https://filtergraph.com/kelt\\$_\\$vars](https://filtergraph.com/kelt$_$vars).

TABLE 6
ROTATION INFORMATION FOR TIC DWARF CANDIDATES

2MASS ID	TIC-ID	V	T_{EFF} [K]	$\log(g)$ [cgs]	Period [d]	False Alarm	Power	Variability Flag
J00045990+2333149	258866603	11.996	5919	4.319	1.141100	0.000	37.068	1
J00085571+3042200	283863167	12.561	5416	4.417	1.372040	0.000	86.530	1
J00111622+2536432	437738492	12.309	5297	4.441	0.693178	0.000	85.164	1
J00135824+2837082	437745995	—	—	—	0.749777	0.000	181.964	1
J00140260+4359337	440050971	11.661	6196	4.270	0.778677	0.000	25.398	1
J00141121+4359070	440050964	11.317	5829	4.336	0.639223	0.000	70.911	1
J00142250+4153311	440060221	11.947	6367	4.949	1.344650	0.000	83.455	1
J00170218+3527076	365965666	11.657	5709	4.358	0.904945	0.000	66.687	1
J00200694+3313517	57963765	12.050	6071	4.292	0.822423	0.000	29.616	1
J00210702+2847497	437750603	11.261	6525	4.220	0.789634	0.000	38.458	1
J00211918+3524154	58017347	10.943	6367	4.243	0.515568	0.000	1239.500	1
J00214490+2454586	437752383	10.918	6331	4.248	1.691390	0.000	126.025	1
J00214996+2455562	437755602	11.541	5724	4.355	1.691390	0.000	81.200	1
J00215799+2529191	437755446	12.016	6219	4.266	0.638818	0.000	19.568	1
J00272000+3202265	44452888	11.260	6297	4.254	0.523314	0.000	380.715	1
J00272759+2650132	440657189	11.330	4736	4.374	0.599395	0.000	62.237	1
J00281478+4315406	190997597	10.525	—	—	0.962733	0.000	51.365	1
J00303360+3927228	115513521	11.971	6122	4.283	4.505320	0.000	111.225	1
J00305701+4310093	191132800	12.328	5488	4.402	1.849320	0.000	665.388	1
J00330646+2212252	242745294	10.608	6608	4.209	0.775092	0.000	219.715	1

NOTE. — *: This is only a part of the full table to be released online. The Variability flag denotes if the stellar rotation period was also recovered as part of the variability search. The most up-to-date version of this table, including updates from new versions of the TIC, additional KELT observations or improved selection metrics is available for download at the *Filtergraph* portal [https://filtergraph.com/kelt\\$_\\$vars](https://filtergraph.com/kelt$_$vars).